Molecular Therapy
Nucleic Acids
Original Article

miR-15a/-16 Inhibit Angiogenesis by Targeting the Tie2 Coding Sequence: Therapeutic Potential of a miR-15a/16 Decoy System in Limb Ischemia

Marie Besnier,[1,6] Saran Shantikumar,[1,7] Maryam Anwar,[2] Parul Dixit,[2] Aranzazu Chamorro-Jorganes,[2] Walid Sweaad,[2] Graciela Sala-Newby,[1] Paolo Madeddu,[1] Anita C. Thomas,[1] Lynsey Howard,[1] Sobia Mushtaq,[1,8] Enrico Petretto,[3,4] Andrea Caporali,[1,5] and Costanza Emanueli[1,2]

[1]Bristol Heart Institute, University of Bristol, Bristol, UK; [2]National Heart and Lung Institute, Imperial College London, London, UK; [3]Institute of Clinical Sciences, Imperial College London, London, UK; [4]Cardiovascular & Metabolic Disorders Programme, Centre for Computational Biology, Duke NUS Medical School, Singapore, Singapore; [5]BHF Centre for Cardiovascular Science, University of Edinburgh, Edinburgh, UK

MicroRNA-15a (miR-15a) and miR-16, which are transcribed from the *miR-15a/miR-16-1* cluster, inhibit post-ischemic angiogenesis. MicroRNA (miRNA) binding to mRNA coding sequences (CDSs) is a newly emerging mechanism of gene expression regulation. We aimed to (1) identify new mediators of the anti-angiogenic action of miR-15a and -16, (2) develop an adenovirus (Ad)-based miR-15a/16 decoy system carrying a luciferase reporter (Luc) to both sense and inhibit miR-15a/16 activity, and (3) investigate *Ad.Luc-Decoy-15a/16* therapeutic potential in a mouse limb ischemia (LI) model. LI increased miR-15a and -16 expression in mouse muscular endothelial cells (ECs). The miRNAs also increased in cultured human umbilical vein ECs (HUVECs) exposed to serum starvation, but not hypoxia. Using bioinformatic tools and luciferase activity assays, we characterized miR-15a and -16 binding to Tie2 CDS. In HUVECs, miR-15a or -16 overexpression reduced Tie2 at the protein, but not the mRNA, level. Conversely, miR-15a or -16 inhibition improved angiogenesis in a Tie2-dependent manner. Local *Ad.Luc-Decoy-15a/16* delivery increased Tie2 levels in ischemic skeletal muscle and improved post-LI angiogenesis and perfusion recovery, with reduced toe necrosis. Bioluminescent imaging (*in vivo* imaging system [IVIS]) provided evidence that the *Ad.Luc-Decoy-15a/16* system responds to miR-15a/16 increases. In conclusion, we have provided novel mechanistic evidence of the therapeutic potential of local miR-15a/16 inhibition in LI.

INTRODUCTION

Peripheral artery disease affects 20% of individuals over 70 years of age worldwide[1,2] and can result in critical limb ischemia (CLI), a debilitating condition characterized by pain at rest, tissue loss, and gangrene. The current management of CLI involves revascularization of the affected limb by percutaneous angioplasty or surgical bypass. However, many CLI patients are not suitable for revascularization for reasons such as severe comorbidities or late diagnosis. In approximately 30% of severely affected patients, minor or major amputations are inevitable.[3] Novel therapeutics to locally promote angiogenesis, and hence reperfusion, would help to overcome a significant unmet clinical need.

Historically, human clinical trials have been informed by pre-clinical studies based on the delivery of single proangiogenic growth factors of the vascular endothelial growth factor (VEGF) and fibroblast growth factor (FGF) families.[4,5] Such approaches have not yet yielded the desired results.[6,7] To reach the bedside of CLI patients, angiogenic therapies require further refinement, including revisiting the realm of therapeutic targets and their mechanisms of action.[8]

MicroRNAs (miRNAs) are small non-coding RNAs that, in their mature form, act at the post-transcriptional level by targeting multiple mRNAs.[9] miRNAs are transcribed as a primary transcript (pri-miRNA) from miRNA genes or intronic regions of protein-coding genes, and they are subsequently processed to reach their mature and functional status.[10] The initial and canonical model of miRNA-induced mRNA-silencing activity relies on semi-complementary binding between the miRNA seed sequence of 7 nt to miRNA-binding sequences contained in the 3′ UTR) of target mRNAs. However, it is becoming increasingly evident that miRNA binding to the 5′ UTR and coding sequences (CDSs) of mRNAs have powerful functional consequences.[11] Each miRNA can target up to several hundred genes

Received 19 October 2018; accepted 5 May 2019;
https://doi.org/10.1016/j.omtn.2019.05.002.

[6]Present address: Lowy Cancer Research Centre, University of New South Wales, Sydney, NSW, Australia.

[7]Present address: Warwick Medical School, University of Warwick, Coventry, UK.

[8]Present address: Department of Biochemistry, PMAS Arid Agriculture University, Rawalpindi, Pakistan.

Correspondence: Costanza Emanueli, National Heart and Lung Institute, Imperial College London, ICTEM building - level 4, Hammersmith Campus Du Cane Road, London W12 0HH, UK.
E-mail: c.emanueli@imperial.ac.uk

and multiple pathways, and miRNAs are known to be involved in the regulation of a plethora of cellular processes, including angiogenesis.[12] Additionally, functionally active miRNAs are released from parent cells and taken up by bordering and possibly distant cells,[13] where they can repress their target genes, thus providing a widespread method of gene expression regulation. Investigations based on individual miRNA experiments have identified miRNAs with either proangiogenic or anti-angiogenic effects.[14,15]

miR-15 and miR-16 are organized in two different clusters, miR-15a/16-1 and miR-15b/16-2, and they are conserved between humans and mice.[16] The sequences of mature miR-15a and miR-15b differ by 4 nt,[16] while miR-16-1 and miR-16-2 have the same mature sequence and, hence, are commonly indicated as miR-16. miR-15a/b and -16 belong to the miR-16 family consisting of miR-15a, miR-15b, miR-16, miR-195, miR-424, and miR-497. The family is extendable to miR-103, miR-107, miR-646, and miR-503, due to homologies in the seed sequences.[17] The extended miR-16 family is involved in angiogenesis regulation: miR-16 targets VEGF receptor 2 and FGF receptor 1, thus decreasing the proangiogenic activity of their ligands.[18] Moreover, following LI, therapeutic angiogenesis is impaired in mice with *miR-15a* gene knockin.[19] We previously described that miR-15a and -16 are increased in both the proangiogenic circulating cells (PACs) and the serum of CLI patients (versus healthy subjects). We also showed that serum concentrations of miR-15a and miR-16 predict the need for amputation at 1 year from revascularization in CLI subjects.[20] In further support of the relevance of miR-15a and miR-16 in the CLI setting, we provided evidence that *ex vivo* transfection with miR-15a/16 inhibitors increases the potential of human PACs to induce therapeutic angiogenesis in an immunocompromised mouse LI model.[20]

Among the different ways to inhibit miRNA, the use of miRNA decoys or sponges that consist of multiple specific miRNA-binding site sequences inserted downstream of a reporter gene represents a promising approach.[21–24] Using a decoy for the diabetes-associated miR-503, we have already provided proof of concept that adenovirus (Ad)-mediated local delivery of a miRNA decoy can improve post-ischemic angiogenesis and blood flow recovery in mice with LI.[23,24] When delivered into cells, the binding of the targeted miRNA to the decoy sequences not only inhibits the miRNA by sequestration but also reduces the expression of the reporter gene used, often EGFP[22] or luciferase.[25] This construct could, therefore, be used as a sensor of the targeted miRNA quantity, as the protein activity of the reporter used is inversely correlated to the presence of the miRNA.[26,27] Additionally, more recent technological advancements allow non-invasive and precise measurement of luciferase activity *in vivo* in mice.[28,29] On these bases, we reasoned that Ad-mediated local delivery of a double miR-15a/16 decoy could provide therapeutic advantages by ensuring release from miRNA inhibition in a spatiotemporally defined window that is supportive of post-ischemic vascular repair.

This study was designed to mechanistically investigate the anti-angiogenic effect of miR-15a/16 and to develop an Ad.miR-15a/16 decoy to be tested for its therapeutic potential, in a mouse LI model.

RESULTS

miR-15 and -16 Expressions in Human and Mouse Tissues

Expressions of miR-15a/b and miR-16 were assessed by qRT-PCR in 19 different human tissues. As shown in Figures 1A–1D, skeletal muscle showed the highest expression of miR-15a and was the tissue with the third highest expression of miR-16, after adipose and prostate tissues. Skeletal muscle was the fifth highest localization of miR-15b and the fourth for miR-503, which we previously found to be increased in diabetic CLI.[23] The relative expressions of the four individual miRNAs in human limb muscles are reported in Figure 1E. Considering these data, we focused the study on miR-15a and miR-16.

To investigate whether miR-15a and -16 expressions are regulated by LI, we harvested mouse adductor and gastrocnemius muscles at 1 and 3 days post-femoral artery ligation or sham operation, and we measured miRNA expression in the whole tissues and in muscle CD146+ microvascular cells. Ischemia-associated expressional changes in the whole muscles were limited to miR-15a (Figure 2A). However, both miRNAs were increased in the ischemic microvascular cells (Figure 2B).

We next moved to model the ischemic environment *in vitro*, by exposing cultured human umbilical vein endothelial cells (HUVECs) to either oxygen or nutrient deprivation. When combined, hypoxia (1% pO_2) and serum starvation increased the expression of the prototypical hypoxamiRNA proangiogenic miR-210[30] (Figure S1), used here as a positive control to validate the culture conditions. The expression of miR-16 was also increased, while miR-15a was unchanged. Taking each condition separately, hypoxia alone increased miR-210 expression, but it did not affect miR-15a/16 levels (Figures S2A–S2C). By contrast, serum deprivation for 24 h increased the expressions of both miR-15a and -16 (Figures S2D and S2E). As expected, miR-210 expression was unaffected by serum starvation (Figure S2F). As shown in Figure S3, the serum starvation-induced expressional changes were limited to the mature forms of miR-15a and -16, and neither the primary transcript (pri-miR-15a/16-1) nor the individual miRNA precursors (pre-miR-15a, pre-miR-16-1, and pre-miR-16-2) were affected.

miR-15a and -16 Target Tie2 in CDS, and Tie2 Repression Mediates the Anti-angiogenic Responses to miR-15a and -16

miR-16 has already been shown to inhibit the angiogenic potential of HUVECs.[18] Using a 2D Matrigel assay, we have confirmed these data and additionally characterized that miR-15a inhibits angiogenesis *in vitro* (Figure S4). Next, we set out to investigate the miRNA putative target genes that could elucidate the anti-angiogenesis response. In previous studies, bioinformatic predictions assuming miRNAs targeting the 3′ UTR of mRNAs have identified VEGF-R2, FGF-R1, VEGF-A, FGF-1, FGF-2, and AKT-3 to be repressed by miR-15/16.[18,20,31,32] More recently, members of the miR-16 family have been shown to bind in the CDS region of their targeted

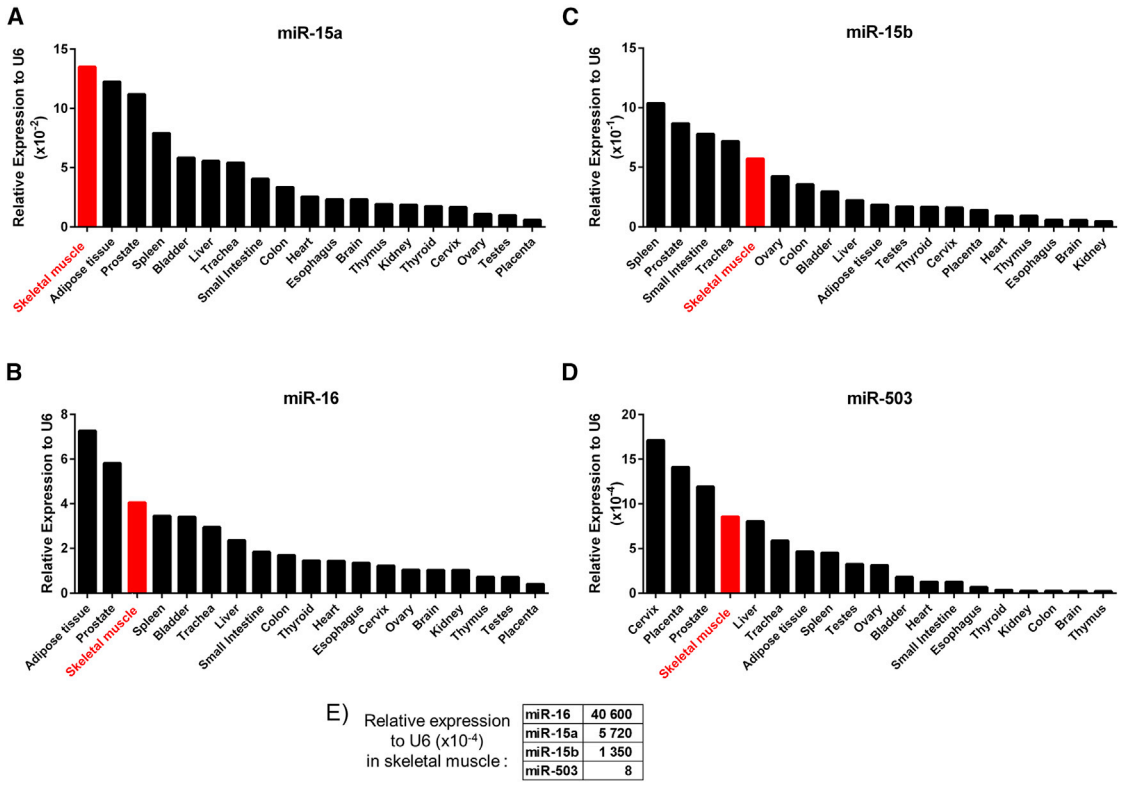

E)

Relative expression to U6 (x10-4) in skeletal muscle :	
miR-16	40 600
miR-15a	5 720
miR-15b	1 350
miR-503	8

Figure 1. miR-15a, -15b, -16, and -503 Expressions in Human Tissues

Expressions of miR-15a (A), miR-16 (B), miR-15b (C), and miR-503 (D) in human tissues assessed by RT-PCR and relative expression of each miRNA in skeletal muscle (E). Results were normalized to small nuclear RNA U6 (U6) expression (n = 1/tissue, resulting from the pooling of three different donor samples).

mRNAs.[11,33,34] Therefore, we expanded our search to putative miRNA-binding sites in the CDS of proangiogenic genes. A genome-wide prediction using miRcode revealed 12,269 common targets of miR-15a and -16. To identify gene ontology (GO) terms and processes to which these common targets correspond, a GO enrichment analysis was performed using the program CLUEGO. Overall 48 GO terms were significantly enriched among the common targets of miR-15a and -16. The top 15 of the GO terms for these predicted targets included blood vessel development (Figure S5A).

From this search, TEK (aka, Tie2 angiopoietin receptor) was declared an interesting candidate, because it is one of the most studied regulators of angiogenesis.[35] Four angiopoietin (Ang) ligands can bind to Tie2.[36] Among them, the most studied are Ang1 and Ang2. Ang1 has a clear agonistic impact on Tie2 and promotes angiogenesis and vessel stability. The type of interaction of Ang2 and Tie2 and vascular consequences are more debated and context dependent.[36–38] Ang2 has been reported to increase by inflammatory and hypoxic stimuli and to promote neoangiogenesis.[39] However, Ang2 can also disrupt the connections between the endothelium and perivascular cells and promote cell death and vascular regression.[38,40] We decided to focus on TEK because a closer inspection of the miRcode results revealed that there is only one binding site for miR-15a and -16 in the CDS region of *TEK* and no binding sites in the 3′ or 5′ UTR. This implied that the possible direct regulatory actions of miR-15a and miR-16 on *TEK* are exclusively mediated via miRNA binding in the CDS. In more detail, this single binding site is a 6-bp region, and the exact location is at chromosome (chr)9: 27204938–27204943 (Figure S5B). This site is highly conserved in mammals (83%) followed by primates (67%) and vertebrates (46%) (Figure S5C).

Next, to validate the direct binding of miR-15a or miR-16 to this CDS of Tie2 mRNA, we developed a luciferase reporter assay in which a sequence of 50 nt either side of the predicted binding site of miR-15a/16 on *TEK* (LUC-TEK), or to the same sequence but where the binding site was mutated (LUC-TEKmut), was cloned downstream of luciferase gene (Figure 3A). In HeLa cells carrying LUC-TEK, overexpression of miR-15a and/or miR-16 by pre-miRNA transfection decreased luciferase activity. This response was not observed if cells were carrying LUC-TEKmut (Figure 3A). To obtain evidence of the consequence of Tie2 targeting by miR-15/16 for angiogenesis, we next moved to HUVECs. In HUVECs transfected to overexpress either miR-15a or miR-16 (Figure 3B), Tie2 mRNA expression was increased (Figure 3C), while Tie2 protein level was decreased (Figure 3D), consistent with the notion that miRNA binding to the mRNA CDS leads to RNA translation inhibition.[41] Conversely, inhibition of miR-15a and -16 using anti-miRNAs increased Tie2 protein

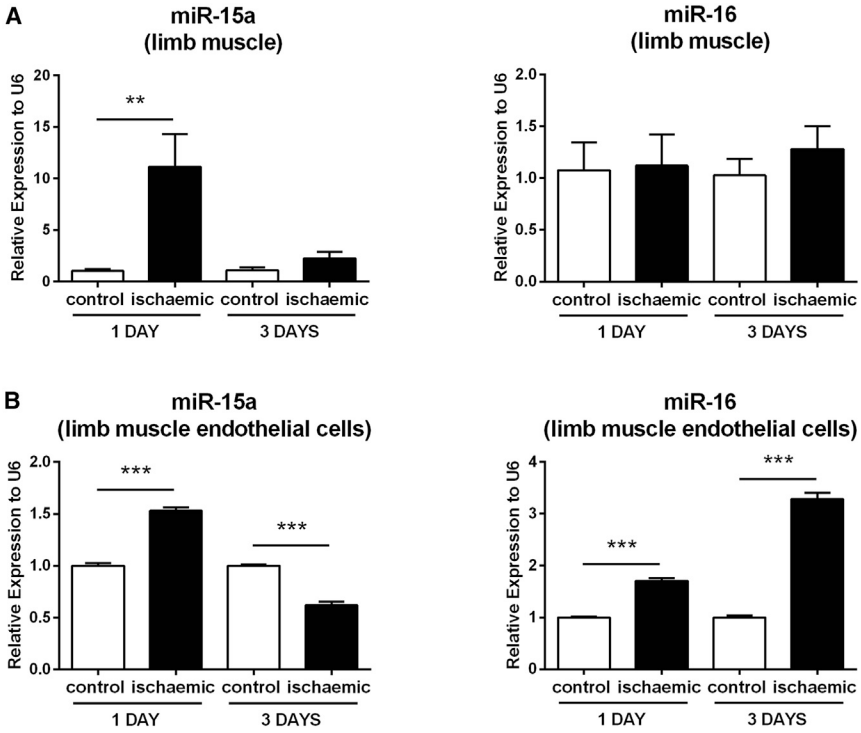

Figure 2. Expressions of miR-15a and -16 Are Differentially Modulated in Mouse Adductor Muscles and Muscle-Derived Endothelial Cells after Limb Ischemia

At 1 and 3 days after surgical induction of limb ischemia, ischemic and contralateral (control) adductor muscles were collected, and the expressions of miR-15a and -16 were assessed by RT-PCR in the total muscle tissue (A) and in muscle-derived CD146+ endothelial cells (ECs) (B). Results were normalized to the expression of small nuclear RNA U6, relative to control muscle or EC normoperfused and expressed as mean ± SEM. n = 3 per condition. **p < 0.01 and ***p < 0.001 versus control, matched for time after ischemia.

expression (Figure 3E). This was associated with a proportional increase in Tie2 phosphorylation, indicating that Tie2 receptors released from the miRNA inhibitory block were functionally active[42] (Figure S6). The importance of Tie2 in mediating the anti-angiogenic effect of either miR-15a or miR-16 was finally confirmed by using a pharmacological inhibitor of Tie2 activity.[43] Tie2 inhibition prevented the proangiogenic response to inhibition of either anti-miR-15a or anti-miR-16 (Figure 3F).

To understand whether the expression of miR-15a and -16 and Tie2 are correlated in ischemic limb muscles and their microvascular cells, we measured Tie2 expression in similar conditions by RT-PCR and by immunohistochemistry. While miR-15a and -16 were increased by ischemia (Figures 2A and 2B), Tie2 protein level was unchanged in ischemic capillaries (Figures S7A–S7H), suggesting that additional molecular mechanisms are responsible for Tie2 expressional regulation. Ang1 expression was not changed in muscles at 1 and 3 days, post-ischemia. By contrast, Ang2 increased at 3 days post-ischemia (Figures S7A and S7B).

Ad.Luc-miR-15a/16 Decoy Can Be Used to Sense Expressional Changes in miR-15a and -16

We next prepared Luc-Decoy in the form of a miRNA decoy system linked to a luciferase reporter gene (Figure S8A), with the intention to both sense changes in endogenous miR-15a and -16 levels and inhibit the functionality of miR-15a/16 in cultured cells and in murine ischemic limb muscles. The capacity of this tool to sequester the endogenous miRNA, thus inhibiting miRNA activity, was already proven in our previous publications on miR-503.[23,24] Here, we additionally evaluated whether *Ad.Luc-miR-15a/16 Decoy* was useful in tracking expressional changes in miR-15a and -16 expression *in vitro* and *in vivo*. We used HeLa cells transfected with either pre-miR-15a or pre-miR-16, and infected with either *Ad.Luc-Decoy* or *Ad.Luc* to validate that increases in intracellular miR-15a and -16 reduce luciferase activity detected in an *in vivo* imaging system (IVIS) apparatus (Figure S8B). Importantly, we could confirm that *Ad.Luc-Decoy* was selectively sensing changes in miR-15a and -16 in comparison with other miR-16 family members, such as miR-15b and miR-503 (Figure S8C).

We next investigated whether the *Ad.Luc-Decoy* system could be used to sense increases in endogenous miR-15a and -16 expressions. To this aim, HUVECs were infected with *Ad.Luc-Decoy* or *Ad.Luc* and submitted to serum withdrawal. After 24 h, we found a decrease in luciferase activity in cells infected with *Ad.Luc-Decoy* in comparison to cells infected with *Ad.Luc* control (Figure 4A). We then evaluated the effect of *Ad.Luc-Decoy* injection into murine muscles after the induction of LI *in vivo*. At 1 day post-LI, in keeping with the increased miR-15a and -16 expressions in total ischemic muscle (see Figure 2A), the luciferase activity was reduced in mice injected with *Ad.Luc-Decoy* compared with mice injected with the control virus (Figures 4B and 4C). A reduction in luciferase activity was also observed at day 21, when miR-16 was found upregulated in ischemic muscle (Figure S9). Figure 4D summarizes the modality of action and potential of *Ad.Luc-Decoy*.

Ad.Luc-Decoy Improves Post-ischemic Blood Flow Recovery and Therapeutic Angiogenesis

We finally provided evidence of the therapeutic potential of *Ad.Luc-Decoy* in the mouse LI model. When compared with *Ad.Luc, Ad.Luc-Decoy* improved post-ischemic blood flow recovery (Figures 5A and 5B) and increased the reparative angiogenesis response in the ischemic muscles (Figures 5C and 5D). The latter was demonstrated by a 35% increase in capillary density (CD31+ capillaries) and 47%

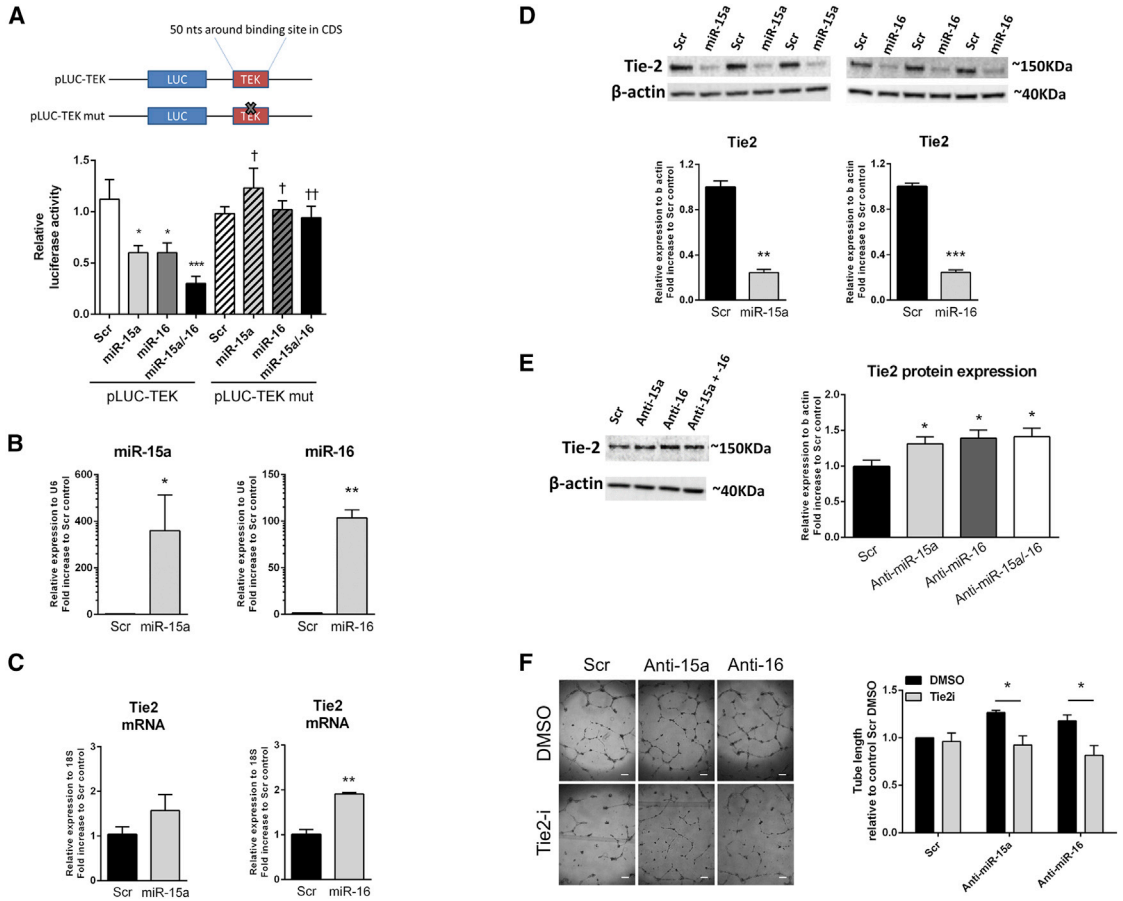

Figure 3. Tie2 Is Targeted by miR-15a and -16 through an Unusual Binding Site on Tie2 mRNA, and It Is Involved in the Proangiogenic Effect of miR-15a and -16 Inhibition in HUVECs *In Vitro*

(A) Luciferase activity at 48 h post-co-transfection of HEK293T cells with pre-miR-15a (miR-15a), pre-miR-16 (miR-16), a combination of the two (miR-15a/16), or miR-scrambled oligonucleotides (Scr) and plasmid containing luciferase open reading frame (pLUC), followed by a portion of 50 nt of the TEK-coding sequence surrounding the putative miRNA-binding site (pLUC-TEK). A mutated version of the miRNA-binding site was used as a control (pLUC-TEKmut). A schematic of the plasmid construct is also provided. *$p < 0.05$, ***$p < 0.001$ versus pLUC-TEK control Scr; †$p < 0.05$, ††$p < 0.01$ versus pLUC-TEK to the pre-miRNA matching condition (n = 5). (B) Human umbilical vein endothelial cells (HUVECs) were transfected with a Scramble oligo (Scr), pre-miR-15a (miR-15a), or pre-miR-16 (miR-16) (5 nM) to increase their respective mature miRNA expression. miR-15a and -16 expressions were assessed by RT-PCR and normalized to small nuclear U6 expression. Tie2 mRNA (C) or protein (D) expressions were assessed by RT-PCR and western blot and normalized to 18S and β-actin, respectively. n = 3 for each condition. (E) HUVECs were transfected with a Scramble oligo (Scr) or an anti-miRNA against miR-15a, miR-16, or the two anti-miRNAs simultaneously (total concentration of 50 nM) to inhibit their activity. Tie2 protein expression was assessed by western blot and normalized to β-actin. n = 9 for each condition. *$p < 0.05$ versus Scr condition. (F) Effect of inhibition of Tie2 on miR-15a/16 inhibition-induced angiogenesis was assessed in HUVECs transfected with a Scramble oligo (Scr) or an anti-miRNA against miR-15a or miR-16 (50 nM) and treated with Tie2 inhibitor (Tie2-I, 5 μM) or DMSO control. The angiogenic capacity was measured by network formation on Matrigel, calculated as total length in millimeters and expressed as a percentage of the Scr and DMSO conditions. Representative pictures are provided (scale bar, 200 μm). n = 3. *$p < 0.05$, **$p < 0.01$, ***$p < 0.001$. All results are expressed as mean ± SEM.

increase in the density of small (lumen diameter <20 μm) arterioles (Figures 5C and 5D) in the ischemic muscles. A similar post-ischemic increase in capillary density was found using Isolectin B4 as a marker for ECs (*Ad.Luc* versus *Ad.Luc-Decoy* at 21 days post-ischemia: 557 ± 69 versus 812 ± 97 capillaries/mm^2 (mean ± SEM).

Using toe necrosis as a marker of ischemia severity,[44] we showed that *Ad.Luc-Decoy* improved toe survival (Figure 5E). Finally, in line with *in vitro* data reported in Figures 3C and 3D, *Ad.Luc-Decoy* increased Tie2 protein expression (Figure 5F), and it did not change the expressions of Tie2 ligands Ang1 and Ang2 (Figure S10). The mRNA expressions of VEGF-A, VEGF- R2, FGF-2, and FGF-1, which were all described to be bound in their 3′ UTRs by miR-15a or -16, were also unchanged (Figure S11).

DISCUSSION

This study has characterized the expressional regulation of miR-15a and -16 in ischemic ECs, and it identified that the anti-angiogenic actions of these miRNAs is in part mediated by the repression of Tie2. Additionally, we have utilized a miRNA decoy approach to sense and

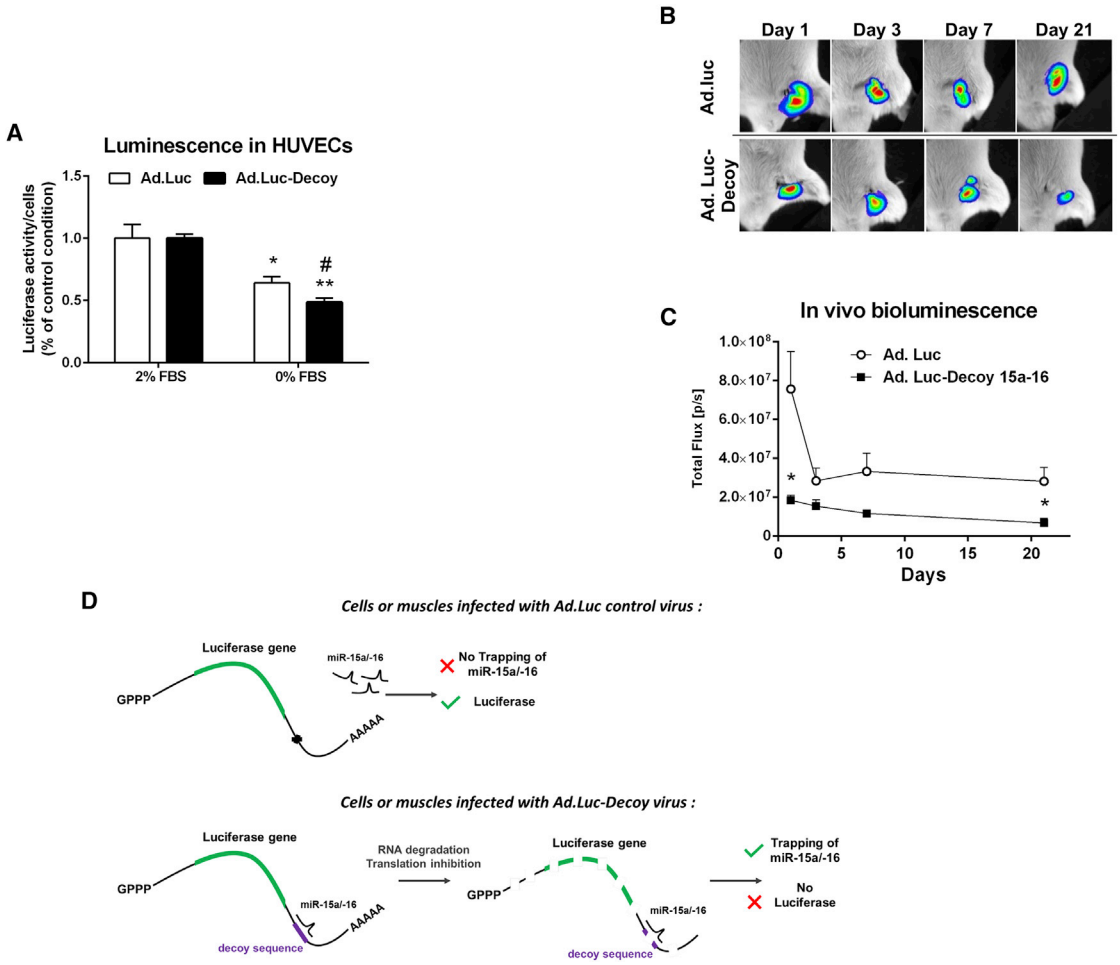

Figure 4. Adenovirus Carrying a Decoy Sequence for miR-15a and -16 (*Ad.Luc-Decoy*) Sensor Activity and Inhibition Efficiency *In Vivo*

(A) Luciferase activity measured on an IVIS of HUVECs infected with *Ad.Luc* control or *Ad.Luc-Decoy* virus cultured under complete (2% FBS) or serum-deprived (0% FBS) media for 24 h. Results are expressed per cell and relative to Ad.-matching, 2% FBS condition. Results are presented as the mean of n = 4–5 per condition ± SEM. *$p < 0.05$, **$p < 0.01$, ***$p < 0.001$ versus Ad.-matching, 2% FBS condition; #$p < 0.05$ versus Ad.-Luc, 0% FBS condition, Student's t test. (B and C) After limb ischemia, bioluminescence activity (expressed as photons per second per centimeter squared per steradian ($P \cdot s^{-1} \cdot cm^{-2} \cdot sr^{-1}$) was measured and analyzed in the ischemic legs using the Xenogen IVIS. D-Luciferin was subcutaneously injected into the ischemic limb, and the consequent bioluminescence from the reaction with the luciferase in either *Ad.Luc*- or *Ad.Luc-Decoy*-injected legs was measured from day 1 to day 21 after injection of the viruses. Representative images are presented. Data are shown as mean ± SEM ($n \geq 10$ per condition). *$p < 0.05$ versus time-matched *Ad.Luc* condition using Student's t test. (D) Schematic explanation of the mechanisms of miR-15a and -16 inhibition, trapping, and sensing in cells expressing the Luc control construct, lacking complementary-decoy sequence for miR-15a/16 or the *Luc-Decoy* construct.

inhibit the activity of endogenous miR-15a and -16 in cultured cells and mouse ischemic muscles. *In vivo* work has provided evidence of the therapeutic potential of *Ad.Luc-Decoy* in CLI.

miR-15a and -16 were previously described to be expressed in various solid and blood cancers.[45,46] Additionally, the group of van Rooij[47,48] has studied miR-15 in the ischemic heart, showing that it induces cell-cycle arrest in neonatal cardiomyocytes and contributes to ischemic damage of the heart in adult rodent and swine models. Early in this study, we found that, under basal conditions and comparing several human organs and tissues, miR-16 and especially miR-15a are more highly expressed in the skeletal muscle compared to the heart. To the best of our knowledge, the consequences of endogenous changes in miR-15a and -16 in LI, and their possible impact on post-ischemic vascular responses, have never been directly investigated. However, we previously reported increased serum levels of miR-15a and -16 in diabetic CLI patients, where circulating miR-15a and -16 levels were able to predict clinical outcome (amputation) at 12 months post-revascularization.[20] In this new study, we have been able to show that LI increases miR-15a and -16 in the muscular microvascular cells and that the ischemia-induced increases in these endogenous miRNAs impair post-ischemic vascular repair, worsening blood flow recovery and toe survival.

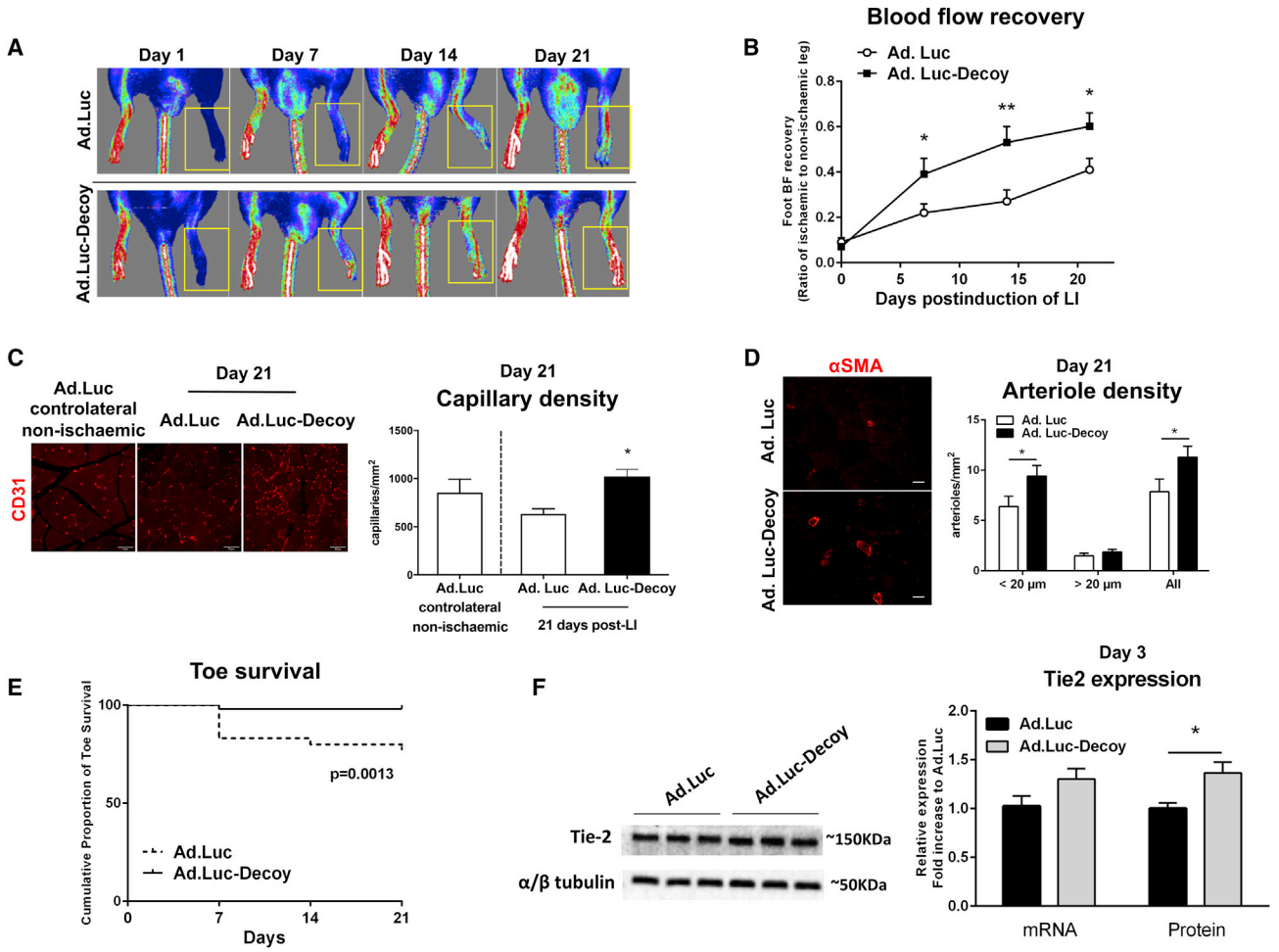

Figure 5. Inhibition of miR-15a/16 Improves Blood Flow (BF) Recovery, Post-ischemic Neovascularization, and Toe Survival following Limb Ischemia

Limb ischemia was induced in mice by femoral artery ligation, and *Ad.Luc* or *Ad.Luc-Decoy* was injected into the ischemic adductor muscle immediately after surgery. (A and B) Line graph shows the time course of post-ischemic BF recovery (calculated as the ratio between the BF of the ischemic foot and the contralateral foot) in mice injected with *Ad.Luc* or *Ad.Luc-Decoy*. Representative color laser Doppler images taken at days 0, 7, 14, and 21 post-ischemia are provided. Yellow frames show the ischemic foot analyzed. Data are presented as mean ± SEM (n ≥ 10 per group). *p < 0.05, **p < 0.01 versus time-matched *Ad.Luc* condition. (C) Immunohistological analysis and representative microphotographs showing the capillary density in mice injected with *Ad.Luc* or *Ad.Luc-Decoy* 21 days after LI and in contralateral (control) muscle of mice injected with *Ad.Luc* (n = 5 per group), assessed by immunolabelling of CD31 as a marker of endothelial cells. Scale bar, 50 µm. (D) Immunohistological analysis and representative microphotographs showing arteriolar density in mice injected with *Ad.Luc* or *Ad.Luc-Decoy* (n = 11 or 8 mice per group, respectively) after limb ischemia, assessed by immunolabelling of α-smooth muscle actin (αSMA) as a marker of vascular smooth muscle cells. Arterioles were quantified according to vessel diameter (<20 µm or ≥20 µm). Data are presented as mean + SEM. Scale bar, 20 µm. (E) Cumulative proportion of toe survival over 21 days of follow-up after ischemia in mice injected with *Ad.Luc* or *Ad.Luc-Decoy* (n ≥ 10 mice per group). p = 0.0013, log rank test. (F) Tie2 expression in ischemic adductor muscles, 3 days after limb ischemia surgery and injection with either *Ad.Luc* or *Ad.Luc-Decoy* virus, was assessed at mRNA and protein levels by RT-PCR and western blot, respectively. Results were normalized to GAPDH for mRNA analysis (n = 6) or to α/β-tubulin for protein analysis (n = 9) and presented as mean ± SEM. *p < 0.05 versus *Ad.Luc* group.

It should be noted that, under our ethics license, we are not allowed to study more severe forms of LI outcome, and we must humanely euthanize our research animals if these occur. The angiogenic response observed in mice after local delivery of *Ad.Luc-Decoy* is in line with our previous work on human PACs, which were shown to carry higher miR-15a and -16 levels when obtained from CLI patients. Moreover, PACs improved their proangiogenic profile when *ex vivo* simultaneously transfected with inhibitors for the two miRNAs before their efficacy testing in immunosuppressed mice with LI.[20] Similar to the LI setting, miR-15a is elevated in the ischemic heart.[48] In contrast, hypoxic cancer tissues expressed less miR-15a/miR-16 than non-hypoxic ones.[49] miR-15/16 function as a tumor suppressor by targeting BCL2.[45] They also inhibit cancer angiogenesis by targeting FGF-2.[49] Therefore, in cancer, miR-15/16 expression deregulation might contribute to explaining why hypoxia, a common micro-environmental feature of rapidly growing tumors, is associated with worse clinical outcomes.[50] According to our data, in ischemic non-cancerous ECs, the regulation of miR-15a and -16 expression is

hypoxia independent and triggered by nutrient deprivation. We have also clarified that increases in mature miR-15a and -16 are not associated with equivalent changes in primary or precursor miRNA expression and, hence, are possibly due to either slower miRNA decay or accelerated maturation of the pre-miRNAs to mature miRNAs.

This study has newly identified Tie2 as a target of miR-15a and -16. The angiopoietin Tie2 receptor is mainly expressed in the vascular endothelium and involved in embryonic and post-natal blood vessel development.[51,52] Interestingly, we found that Ang2 was upregulated in ischemic muscles, while Ang1 was unchanged. Tie2 levels were also unchanged by ischemia.

The modality of action of Ang2 on Tie2 is still debated, and it has been suggested to function as a context-dependent agonist or antagonist[42] and to be associated with inflammatory responses.[53] Direct intramuscular injection of plasmid DNA encoding Ang1, but not Ang2, was shown to augment revascularization in a rabbit ischemic hindlimb model.[54] Increasing the Ang1/Tie2 signaling in ischemic limb muscles could be beneficial for reparative angiogenesis.

In fact, Tie2 disruption was shown to impair post-ischemic regeneration in mice with LI.[55] This is in line with our data showing that an *Ad.Luc-Decoy*-induced increase in limb Tie2 is associated with improved post-ischemic reparative angiogenesis and blood flow recovery. We have clarified that miR-15a/16 bind to the CDS of Tie2. A few studies have started to report efficient targeting of miRNAs on CDS. The canonical mechanism of action of a miRNA involves the stabilization of mature miRNA by Argonaute-2 (Ago2) proteins, functioning to direct the RISC (RNA-induced silencing complex) to target mRNAs. According to this model, binding between the miRNA seed sequence to one or more semi-complementary regions within the mRNA 3′ UTR induces post-transcriptional inhibition, manifesting as reduced mRNA and protein levels.[11] It is progressively emerging that this model is probably insufficient to explain miRNA actions and that, in some cases, the most predominant Ago2:miR-binding sites may be found within the CDS.[11]

It has already been shown that miR-103 and -107, which belong to the wider miR-16 family, do make ample use of CDS targeting.[34] The miRNA target sites in the CDS are under evolutionary selection.[41] Sequence conservation has usually been taken as evidence of functional importance.[56,57] In this context, it is of interest that the miR-15a/16-binding sites to CDS targets are conserved between species (human and macaque[58]). miR-15a/b and -16 contain the AGCAGC motif at the 5′ end. Using computational analyses, Hausser et al.[41] found that miRNAs with this motif location have more complementary sites in the CDS compared with 3′ UTR. Such miRNAs also have in common the capacity to regulate the cell cycle.[41] Hausser et al.[41] additionally suggested that CDS binding is more potent in inhibiting mRNA translation, as compared to mRNA degradation. This is consistent with our finding that pre-miR-15a or -16 transfection of HUVECs reduced protein and increased mRNA expression for Tie2.

In our study we used a homology-of-sequence strategy to identify miR-15a and -16 mRNA targets. miRNA-mRNA interactions are largely based on sequence homology, but they are also dependent on additional factors. As an example, mRNA 3D configuration can affect the accessibility of the RISC-binding site.[59] Increasing evidence shows that binding of a miRNA to its mRNA targets can be cell type and environment dependent[60] and that this can be relevant for anti-miRNA cardiovascular therapies.[61] This was already exemplified by Eding et al.,[61] who found that, upon *in vivo* inhibition of the cardiomyocyte-specific miR-208a, the quality and quantity of direct targets of miR-208a that are expressionally modulated depend on the presence and type of cardiac stresses, such as hypertension or myocardial infarction. The anti-miR-208 treatment in healthy and diseased hearts revealed 3 subsets of targets: (1) health-specific targets, (2) disease-specific targets, and (3) targets common to health and disease. In line with that, we have also noted a context-dependent target regulation after the inhibition of miRNA-15a and -16. In fact, Chamorro-Jorganes et al.[18] showed that miR-16 regulates VEGFR2 in human ECs cultured under normal conditions. In our model of LI, miR-15a/16 inhibition using the *Ad.Luc-Decoy* virus did not change the expression of VEGF-R2 or other previously described targets of miR-15a or -16, such as VEGF-A, FGF-1, and FGF-2.[18,20,32]

We have shown that viral vector-mediated local delivery of a miRNA decoy increases the density of small arterioles, which contain vascular smooth muscle cells (VSMCs) and play an important role in the resistance of blood flow in skeletal muscles.[62,63] The data presented here are consistent with our previous report that miR-15a decreased human VSMC migration and proliferation *in vitro*,[20] biological process involved in arteriole growth.[64]

Our study also showed the potential of using a bioluminescence IVIS apparatus to non-invasively detect changes in endogenous miRNA expression in wild-type animals. Conventional techniques to measure miRNA expression usually consist of RT-PCR, microarray analyses, and northern blots. Even though these techniques are accurate, they require lysed cells or tissues that represent a further constraint for time course studies, especially *in vivo*.[65] A major strength versus genome editing of small animal models, which is otherwise possible, is that, once optimized, it can be translated for use in large animal models and human patients. In future studies, the prototypical *Ad.Luc-Decoy* can be refined to increase precision of measurements of different miRNA types, and it can be adapted for use with different viral vectors, with different tropism and length of transgene expression.

Finally, this study has provided the first evidence that local inhibition of miR-15a/16 is effective at improving post-ischemic vascular repair in limbs. This finding has translational implications, and it significantly expands on what has already been reported by Hullinger et al.[48] in heart ischemia models, where locked nucleic acid (LNA)-modified anti-miRNA was employed to target miR-15, reducing infarct size. Hullinger et al.[48] focused exclusively on the heart and did not investigate the vascular response to miRNA inhibition.

Clinical trials based on LNA have already started in patients with different forms of lymphoma and leukemia (https://www.cancer.gov/about-cancer/treatment/clinical-trials/intervention/lna-based-antimir-155-mrg-106). Additionally, gene therapy clinical trials to test proangiogenic therapies have been already authorized by regulatory authorities.[66] Therefore, our proof of concept that miR-15a/16 inhibition holds therapeutic potential in the setting of LI has the potential to be progressed through the translational pipeline via at least two alternatives (LNA or viral vector-mediated Decoy transfer) to reach the bedside of CLI patients.

MATERIALS AND METHODS

Human RNA Tissue Bank Real-Time qPCR Analysis

RNA from a human tissue bank (resulting from the pooling of three samples from different patients) was obtained from Ambion, Applied Biosystems. Reverse transcription was performed using the TaqMan MicroRNA Reverse Transcription kit (Applied Biosystems, 4366596), and real-time PCR was performed in triplicate using the TaqMan universal master mix with the LightCycler480 qPCR detection system (Roche, 04707516001).

Expression was normalized to the small nucleolar RNA U6 (snRU6). Primer identification numbers are indicated in Table S1. Relative miRNA expression was defined from threshold cycle (Ct) values, calculated using the $2^{(-\Delta\Delta Ct)}$ method.

Mouse LI Model

The experiments involving mice were performed in accordance with the Guide for the Care and Use of Laboratory Animals prepared by the Institute of Laboratory Animal Resources and with the prior approval of the UK Home Office and the University of Bristol ethics committee.

Sample size was determined using a power calculation with blood flow at 21 days post-ischemia, measured using laser Doppler, as the primary outcome. Specifically, for an 80% power at a 5% significance level, to detect a 50% increase in ischemic:contralateral limb blood flow ratio (see below) in the test group (from a mean of 0.4 to 0.6, based on previous experience), at least 12 mice were required in each group. Based on our own pilot data on the use of *in vivo* bioluminescence analyses, this number of mice would give us a 90% power to detect a 3-fold difference in bioluminescence activity.

Left LI was induced in 10- to 12-week-old CD1 male mice (Charles River Laboratories, Margate, UK). Mice were anesthetized (tribromoethanol, 880 mmol/kg intraperitoneally [i.p.], Sigma-Aldrich, T48402), and the left femoral artery was ligated with a 6-0 silk suture at two points, followed by electrocoagulation of the ligated segment, leaving the femoral vein and nerve untouched.[67] Analgesia (Vetergesic, 0.02 mL/30 g animals) was administrated after surgery. Mice were excluded and humanely euthanized where they developed signs or symptoms of severe LI, as per the conditions of our ethics license. Any data accrued for excluded mice were still analyzed up to the point of exclusion.

In vivo experiments were performed by three investigators (S.S., L.H., and A.C.T.). Where experiments involved the randomization of mice into one of two groups, the operator and outcome assessor were blinded as to the group allocation. For evaluation of miR-15a/16 expression in ischemic muscles, mice were sacrificed at 1 and 3 days after surgery. Ischemic and contralateral adductor muscles were harvested, and RNA extraction was performed on either the total muscle or muscle $CD146^{+}$ microvascular cells extracted following a previously described protocol.[68]

RNA Extraction from Mouse Tissue and Cells and Real-Time qPCR Analysis

Total RNA was extracted from adductor muscle tissues and mouse cells using miRNeasy Mini 343 Kit (QIAGEN, 217004), according to the manufacturer's instructions. RT-PCR was performed in triplicate as described above.

Cell Culture

HUVECs (Lonza, Slough, UK, CC-2519) were cultured between passages 2 and 6 at 37°C with 5% CO_2 in EBM-2 EC basal medium (Lonza, CC-3156), with the addition of the SingleQuot Kit (EGM-2 medium, Lonza, CC-4176) containing 2% fetal bovine serum (FBS, included in the kit). For hypoxia experiments, cells were exposed to 1% pO_2 for 24 and 48 h, whereas for the normoxia control condition cells were exposed to 21% pO_2. For the serum deprivation condition experiments, cells were cultured in EGM-2 medium without FBS for 24 and 48 h, whereas in the control condition cells were exposed to complete medium. HeLa cells were maintained in DMEM (Invitrogen) supplemented with 10% FBS and 1% penicillin/streptomycin (Gibco, 15140122). Cells were incubated in a humidified atmosphere at 37°C with 5% CO_2.

Bioinformatic Prediction of New miR-15a and -16 Targets

The program miRcode (http://www.mircode.org/index.php) was used to predict common genome-wide targets of miR-15a and miR-16 by looking for their binding sites in the 3′ UTR, 5′ UTR, and CDS regions of human genes. The predicted common targets of the two were then subjected to a GO analysis to identify enriched terms and processes. GO analysis was performed using CLUEGO,[69] with significant terms considered at a Bonferroni-corrected p value of ≤ 0.05.

Luciferase Assay for the Validation of miR-15a and -16 Binding to Tie2 mRNA

The binding sequence for the miR-16 family on Tie2 CDS was identified using miRcode software. The binding site is in position chr9: 27204938–27204943. At 450 bp to either side of the binding site was cloned in pMIR-Reporter (Life Technologies). Primers used for the cloning were as follows: Tie2 CDS, forward 5′-ATAGTGGT TAGGTGGCAGGG-3′ and reverse 5′-CTGCCTGTACTTGGACT TGC-3′. Primers for 3′ UTR mutation were as follows: Tie2 CDS, forward 5′-AGGGGGGAAGAATAATAAATTAGCCATCC TTGG-3′ and reverse 5′-CCAAGGATGGCTAATTTATTATTCTTC CCCCCT-3′.

Luciferase assays were performed as previously described.[24] Briefly, luciferase constructs were transfected into HEK293T cells together with miR-15 and/or miR-16 mimics or p-SV-β-gal control vector. Cells were cultured for 48 h and assayed with the Luciferase and β-Galactosidase Reporter Assay Systems (Promega, E1500 and E2000, respectively). Luciferase values were normalized to protein concentration and β-galactosidase activity.

Tie2 Expression Regulation by miR-15a and -16 in HUVECs

HUVECs were plated on a 6-multiwell plate at a density of 2.0×10^5 cells per well in 2 mL EGM-2 and grown for 24 h until 70%–80% confluent. Cells were then washed once with PBS and maintained in OPTIMEM (Invitrogen, 31985062) for 0.5 h prior to transfection with pre-miRNAs (hsa-miR-15a-5p, PM10235; hsa-miR-16-5p, PM10339, Ambion, 5 nM), anti-miRNAs (MH10339 and MH10235, Ambion, total 50 nM), or a scramble (Scr) control (Cy3 dye-labeled Pre-miR Negative Control, AM17120 or Anti-miR Negative Control AM17011, Ambion) using Lipofectamine RNAiMAX (Invitrogen, 13778150), according to the manufacturer's protocol. At 2 days after transfection, cells were lysed either in ice-cold Pierce radioimmunoprecipitation assay (RIPA) buffer (Thermoscientific, 89900) completed with cOmplete Protease Inhibitor Cocktail (Roche, 11697498001) and phosphatase inhibitor PhosSTOP (Roche, 4906845001) for protein extraction or with QIAzol for RNA extraction (miRNeasy Mini Kit, 217004).

For reverse transcription, cDNA was synthesized from 500 ng total RNA using the QuantiTect RT kit (QIAGEN, Manchester, UK, 205314), as per the manufacturer's instructions, including a step to remove genomic DNA. All cDNA was stored at −20°C. qPCR was performed using Power SYBR (Life Technologies, Paisley, UK, 4368708) with a QuantStudio 6 Flex Real-Time PCR System (Thermo Fisher Scientific), according to the manufacturer's instructions. Primers used to measure the expression of human Tie2 are indicated in Table S2. Data were normalized to 18S as an endogenous housekeeping gene, and relative expression n was calculated using the $2^{-(\Delta\Delta CT)}$ method. To extract protein, lysates were incubated at 4°C on a rotator. Samples were centrifuged at 14,000 × *g* for 15 min at 4°C, and the supernatant fractions were used for western blot. Protein concentration was determined using the Pierce BCA Protein Assay Kit (Thermo Fisher Scientific, 23225). Detection of proteins by western blot analyses was done using 10 μg protein extract on SDS-polyacrylamide gels.

Proteins were transferred to nitrocellulose membranes and probed with the following antibodies: Goat anti-human Tie2 (R&D Systems, AF313, 1:1,000), Rabbit anti-human/mouse phospho-Tie2 (Y992) (R&D Systems, AF2720, 1:3,000), and mouse and human β-actin (Sigma, A5441; 1:50,000). Secondary antibodies used were enhanced chemiluminescence (ECL) mouse immunoglobulin G (IgG) (GE Healthcare, NA931; 1:5,000), mouse anti-goat- horseradish peroxidase (HRP) (Santa Cruz Biotechnology, sc-2354, 1:2,000), and donkey anti-rabbit-HRP (Santa Cruz Biotechnology, sc-2313, 1:2,000). Membranes were stripped between imaging of phospho-Tie2 and total Tie2.

Matrigel Assay of HUVECs Transfected with miR-15a and miR-16 Inhibitors and Tie2 Inhibition

HUVECs were transfected using Lipofectamine RNAiMAX (Invitrogen, 13778150) and anti-miRNA negative control or anti-miR-15a or miR-16 inhibitors, following the protocol described above. The cells were used for Matrigel assay at 48 h after transfection. On the day of the Matrigel assay, HUVECs were plated onto duplicate wells containing 70 μL Reduced Growth Factors Matrigel (BD Biosciences, 356231), on a 96-well plate (10^4 cells/well) in complete medium with or without 5 μM Tie2 inhibitor (ab141270, Abcam) or the equivalent volume of the inhibitor diluent (DMSO, final concentration 0.05%). The experiment continued for 24 h before imaging each well at 5×. Network formation was quantified in randomly captured microscopic fields by calculating the length of cellular network using Image-Pro plus software.

Ad.Luc-Decoy

The fragment of firefly luciferase-decoy 15-16 (Luc-Decoy) under the control of the cytomegalovirus (CMV) promoter (2,662 bp) was excised from TW-3′ UTR LUC DEC15-CYAN[70] with ClaI and EcoRV, blunt ended using mung bean nuclease and ligated into pDC511 shuttle vector (Microbix Biosystems, Canada). Replication-deficient E1-E3-deleted adenovirus was generated by recombination in 293 cells.[71] The DNA construct consists of the CMV promotor followed by a luciferase gene and tandem sequences complementary to miR-15a and also 80% complementary to miR-16 (decoy sequences), separated by an 18-bp unrelated spacer.[70]

Preparation of HeLa Cells and HUVECs for *In Vitro* Bioluminescence Analyses Using the IVIS System

HeLa cells were seeded on a T75 flask at a density of 8×10^5 cells/flask in 10 mL complete DMEM and grown 24 h until 70%–80% confluent. Cells were then infected overnight with *Ad.Luc-Decoy* virus at 10 MOI in DMEM without FBS. To transfect the cells with miRNA precursors, HeLa cells were plated in duplicate on a 6-well plate at a density of 2.5×10^5 cells/well in 2 mL DMEM 10% FBS and grown for 24 h until 70%–80% confluent. Cells were then maintained in OPTIMEM medium (Invitrogen, 31985062) for 30 min prior to transfection with 25 nM pre-miR-15a, pre-miR-16, or Scr. For luciferase activity measurement, after transfection, HeLa cells were plated in a 96-well plate at a density of 1×10^3, 2×10^3, 4×10^3, 6×10^3, 8×10^3, 1×10^4, 2×10^4, and 3×10^4 cells/well in duplicates. After 12 h, the medium was removed and replaced by 100 μL pre-warmed PBS containing 150 μL/mL D-Luciferin (Caliper LifeSciences, 122796). Luciferase activity was measured 1 min after the addition of the D-Luciferin using an IVIS. The average of n = 2 per condition plated in duplicate was then expressed in units of maximum photons per second per centimeter squared per steradian ($P \cdot s^{-1} \cdot cm^{-2} \cdot sr^{-1}$).

HUVECs were seeded on a 12-well plate at a density of 1×10^5 cells/well in 1 mL complete EGM-2 medium and grown until 70%–80% confluent. Cells were then infected overnight with adenoviruses *Ad.Luc-Decoy* or *Ad.Luc* at 100 MOI in EGM-2 complete medium. The following day, the cells were washed with PBS and the medium

was replaced with normal complete or serum-free EGM-2 medium for 24 h. After luciferase activity measurement (performed as in HeLa cells), HUVECs were then trypsinized and counted. The average of n = 5 per condition was then expressed in units of maximum photons per second per centimeter squared per steradian ($P \cdot s^{-1} \cdot cm^{-2} \cdot sr^{-1}$) per cell.

Preparation of Mice for *In Vivo* Bioluminescence Analyses Using the IVIS System

The sample size for *in vivo* work was based on power calculations. Mice were randomized in two treatment groups (n = 14 mice/group) and underwent LI induction.

Immediately after the procedure, *Ad.Luc-Decoy* or *Ad.Luc* (10^9 plaque-forming units per mouse in a total volume of 30 μL injected into 3 equidistant sites) was delivered into the ischemic adductor muscle. The luciferase activity in the ischemic muscles was evaluated at 1, 3, 7, and 21 days post-surgery using the Xenogen *In Vivo* Imaging System. Following the exclusion criterion stated above, the day 21 analysis included 12 mice in the *Ad.Luc-Decoy* group and 10 in the *Ad.Luc* group. Briefly, after anesthesia induction (tribromoethanol, 880 mmol/kg i.p., Sigma-Aldrich, T48402), the mouse ischemic leg was injected subcutaneously with the reporter probe D-luciferin (Caliper LifeScience, 122796) at 150 mg/kg body weight.

After 10 min, animals were imaged. Bioluminescence was quantified and expressed in units of maximum photons per second per centimeter squared per steradian ($P \cdot s^{-1} \cdot cm^{-2} \cdot sr^{-1}$), as described previously.[72]

Efficacy Testing the Therapeutic Potential of *Ad.Luc-Decoy*

The mice used for the IVIS analyses were tested for post-ischemic blood flow recovery, therapeutic angiogenesis, and clinical outcome in terms of toe necrosis. The superficial blood flow (BF) of the ischemic and contralateral foot was sequentially analyzed, starting immediately after surgery and at 7, 14, and 21 days, using a high-resolution laser color Doppler imaging system (Moor LDI2, Moor Instruments, Devon, UK). The ratio between BF in the ischemic and contralateral foot was calculated and used as an index of percentage BF recovery. At 21 days post-ischemia, mice were perfusion fixed under terminal anesthesia, and adductors were harvested and paraffin embedded for histological and immunohistochemical analyses, as previously described.[67] Toe necrosis occurrence, defined as darkening of the toe followed by loss of the tissue, was evaluated along the LI protocol. The cumulative proportion of toe survival at 7, 14, and 21 days after the induction of LI was calculated, excluding mice that showed symptoms of femoral nerve damage.

Histology and Immunohistochemistry on Muscles

The 4-μm-thick adductor muscle slices were stained using Rabbit anti-mouse/human CD31 (Abcam, ab28364, 1:50) and Donkey anti-rabbit Alexa-647 (Jackson ImmunoResearch Laboratories, 711-605-152, 1:200) to detect ECs and with a Cy3-conjugated rabbit polyclonal anti-α-smooth muscle actin antibody (Sigma, C6198, 1:400) to stain VSMCs, present in arterioles. The slides were then mounted using a mounting medium (Fluoromount G, South Biotech, 0100-01) containing DAPI to stain nuclei. The number of capillary and arterioles per millimeter squared was counted in 10 randomly selected high-power fields (magnification 40×) using a Zeiss inverted fluorescent microscope. The lumen diameter of α-smooth muscle actin-positive arterioles was measured using ImageJ software. Tie2 staining in non-ischemic and ischemic muscles was performed using a mouse anti-mouse/human Tie2 antibody (Abcam, ab24859 [Cl. 16], 1:50) and a goat anti-mouse Alexa-568 (Abcam, ab175473, 1:200) on cryosections. At least 5 fields of 40× magnification using Zeiss AxioObserver inverted fluorescent microscope were used to analyze the percentage of Tie2+/CD31+ capillaries. Intensity of staining of Tie2 within the Tie2+/CD31+ capillaries was analyzed using Fiji software.

Tie2 Expression in Ischemic Skeletal Muscle Injected with *Ad.Luc* and *Ad.Luc-Decoy* Virus

Animals received surgery of LI and were injected into the adductor muscle with 10^9 plaque-forming unit (PFU)/animal with either *Ad.Luc* or *Ad.Luc-Decoy*. At 3 days after surgery, animals were euthanized and ischemic muscles were collected and snap frozen. Tissues were mechanically disrupted either in Qiazol (QIAGEN) for RNA extraction or in RIPA buffer (Thermo Scientific, 89900) completed with cOmplete protease inhibitor cocktail and phosphatase inhibitor PhosSTOP for protein extraction, as described above. Total RNA from adductor muscle tissues was extracted using miRNeasy Mini extraction Kit (QIAGEN, 217004), according to the manufacturer's instructions. For tissues collected at 21 days post-LI, total RNA from formalin-fixed and paraffin-embedded tissue sections was isolated using deparaffinization solution and miRNeasy FFPE Kit (QIAGEN 217504), according to the manufacturer's protocol (deparaffinization solution 19093).

For mRNA analysis, reverse transcription was performed using the QuantiTect Reverse Transcription kit (QIAGEN, 205314), according to the manufacturer's protocols. cDNA was amplified by real-time qPCR. cDNA (equivalent to 1 μg total RNA) was incubated in triplicate with gene-specific primers for mouse Angiopoietin-1, Angiopoetin-2, FGF-2, FGF-1, VEGF-A, VEGF-R2, Tie2, GAPDH, and 18S (sequences presented in Table S2). To extract protein, lysates were incubated at 4°C on a rotator. Samples were centrifuged at 14,000 × *g* for 15 min at 4°C, and the supernatant fractions were used for western blot. Protein concentration was determined using the Pierce BCA Protein Assay Kit (Thermo Fisher Scientific, 23225). Detection of proteins by western blot analyses was done using 30 μg protein extract on SDS-polyacrylamide gels for Tie2 and 120 μg for VEGF-R2. Proteins were transferred to nitrocellulose membranes and probed with the following antibodies: goat anti-mouse/rat Tie2 (R&D Systems, AF762, 1:1,000), rabbit anti-human/mouse VEGF-R2 (Abcam, ab39256), and rabbit anti-mouse α/β-Tubulin (R&D Systems, 2148S, 1:2,000). Secondary antibodies used were mouse anti-goat-HRP (Santa Cruz Biotechnology, sc-2354, 1:2,000) and donkey anti-rabbit-HRP (Santa Cruz Biotechnology, sc-2313, 1:2,000).

Statistical Analysis

Results are presented as mean ± SEM. Tests for statistical significance were conducted using GraphPad Prism (version 6; GraphPad, San Diego, CA).

Comparisons between two groups were performed using Student's t test, with the exception of the analysis of the capillary and arteriole densities for which a Welch's unequal variances t test was used. For comparison among more than two groups, ANOVA followed by a Tukey post hoc test was used. Differences in necrosis outcomes were assessed using the log rank test. Exceptions are indicated in the captions. A p value of <0.05 was interpreted to be statistically significant.

SUPPLEMENTAL INFORMATION

Supplemental Information can be found online at https://doi.org/10.1016/j.omtn.2019.05.002.

AUTHOR CONTRIBUTIONS

Participated in research design: M.B., A.C., and C.E. Conducted experiments: M.B., S.S., M.A., P.D., A.C-J., W.S., G.S-N., A-C.T., L.H., and S.M. Contributed new reagents or analytic tools: G.S-N., P.M., and E.P. Performed data analysis: M.B., S.S., M.A., A.C-J., A.C., and C.E. Wrote or contributed to the writing of the manuscript: M.B. and C.E.

CONFLICTS OF INTEREST

The authors declare no competing interests.

ACKNOWLEDGMENTS

Authors would like to acknowledge the Facility for Imaging by Light Microscopy (FILM) at Imperial College London, which is in part supported by funding from the Wellcome Trust (grant 104931/Z/14/Z) and BBSRC (grant BB/L015129/1); we are grateful to Mr. Stephen Rothery (laboratory manager and senior technician at FILM) for his help with fluorescence imaging and analysis. We also acknowledge some technical help from Dr. Micol Marchetti (University of Bristol). This study was funded through the following (to C.E.): British Heart Foundation grants (BHF) research programme grant "microRNAs from cardiac surgery to basic science – and back?" (RG/15/5/31446), and BHF Chair in Cardiovascular Science (CH/15/1/31199); BHF PhD studentship for S.S. (FS/10/61/28566); and Leducq Foundation transatlantic grant on microRNAs in vascular disease (miRVAD).

REFERENCES

1. Annex, B.H. (2013). Therapeutic angiogenesis for critical limb ischaemia. Nat. Rev. Cardiol. *10*, 387–396.
2. Robless, P., Mikhailidis, D.P., and Stansby, G.P. (2007). Cilostazol for peripheral arterial disease. Cochrane Database Syst. Rev. (1), CD003748.
3. Adam, D.J., Beard, J.D., Cleveland, T., Bell, J., Bradbury, A.W., Forbes, J.F., Fowkes, F.G., Gillepsie, I., Ruckley, C.V., Raab, G., and Storkey, H.; BASIL trial participants (2005). Bypass versus angioplasty in severe ischaemia of the leg (BASIL): multicentre, randomised controlled trial. Lancet *366*, 1925–1934.
4. Gowdak, L.H., Poliakova, L., Wang, X., Kovesdi, I., Fishbein, K.W., Zacheo, A., Palumbo, R., Straino, S., Emanueli, C., Marrocco-Trischitta, M., et al. (2000). Adenovirus-mediated VEGF(121) gene transfer stimulates angiogenesis in normoperfused skeletal muscle and preserves tissue perfusion after induction of ischemia. Circulation *102*, 565–571.
5. Caron, A., Michelet, S., Caron, A., Sordello, S., Ivanov, M.A., Delaère, P., Branellec, D., Schwartz, B., and Emmanuel, F. (2004). Human FGF-1 gene transfer promotes the formation of collateral vessels and arterioles in ischemic muscles of hypercholesterolemic hamsters. J. Gene Med. *6*, 1033–1045.
6. Muona, K., Mäkinen, K., Hedman, M., Manninen, H., and Ylä-Herttuala, S. (2012). 10-year safety follow-up in patients with local VEGF gene transfer to ischemic lower limb. Gene Ther. *19*, 392–395.
7. Zachary, I., and Morgan, R.D. (2011). Therapeutic angiogenesis for cardiovascular disease: biological context, challenges, prospects. Heart *97*, 181–189.
8. Carmeliet, P., and Conway, E.M. (2001). Growing better blood vessels. Nat. Biotechnol. *19*, 1019–1020.
9. Mendell, J.T. (2005). MicroRNAs: critical regulators of development, cellular physiology and malignancy. Cell Cycle *4*, 1179–1184.
10. Ha, M., and Kim, V.N. (2014). Regulation of microRNA biogenesis. Nat. Rev. Mol. Cell Biol. *15*, 509–524.
11. Matkovich, S.J., and Boudreau, R.L. (2018). When Knowing "Enough" May Still Not Be Enough. Circ. Res. *123*, 412–414.
12. Yang, W.J., Yang, D.D., Na, S., Sandusky, G.E., Zhang, Q., and Zhao, G. (2005). Dicer is required for embryonic angiogenesis during mouse development. J. Biol. Chem. *280*, 9330–9335.
13. Caporali, A., Miscianinov, V., Saif, J., and Emanueli, C. (2016). MicroRNA transport in cardiovascular complication of diabetes. Biochim. Biophys. Acta *1861*, 2111–2120, *12 Pt B*.
14. Saif, J., and Emanueli, C. (2014). miRNAs in post-ischaemic angiogenesis and vascular remodelling. Biochem. Soc. Trans. *42*, 1629–1636.
15. Bonauer, A., Carmona, G., Iwasaki, M., Mione, M., Koyanagi, M., Fischer, A., Burchfield, J., Fox, H., Doebele, C., Ohtani, K., et al. (2009). MicroRNA-92a controls angiogenesis and functional recovery of ischemic tissues in mice. Science *324*, 1710–1713.
16. Yue, J., and Tigyi, G. (2010). Conservation of miR-15a/16-1 and miR-15b/16-2 clusters. Mamm. Genome *21*, 88–94.
17. Caporali, A., and Emanueli, C. (2011). MicroRNA-503 and the extended microRNA-16 family in angiogenesis. Trends Cardiovasc. Med. *21*, 162–166.
18. Chamorro-Jorganes, A., Araldi, E., Penalva, L.O., Sandhu, D., Fernández-Hernando, C., and Suárez, Y. (2011). MicroRNA-16 and microRNA-424 regulate cell-autonomous angiogenic functions in endothelial cells via targeting vascular endothelial growth factor receptor-2 and fibroblast growth factor receptor-1. Arterioscler. Thromb. Vasc. Biol. *31*, 2595–2606.
19. Yin, K.J., Olsen, K., Hamblin, M., Zhang, J., Schwendeman, S.P., and Chen, Y.E. (2012). Vascular endothelial cell-specific microRNA-15a inhibits angiogenesis in hindlimb ischemia. J. Biol. Chem. *287*, 27055–27064.
20. Spinetti, G., Fortunato, O., Caporali, A., Shantikumar, S., Marchetti, M., Meloni, M., Descamps, B., Floris, I., Sangalli, E., Vono, R., et al. (2013). MicroRNA-15a and microRNA-16 impair human circulating proangiogenic cell functions and are increased in the proangiogenic cells and serum of patients with critical limb ischemia. Circ. Res. *112*, 335–346.
21. Carè, A., Catalucci, D., Felicetti, F., Bonci, D., Addario, A., Gallo, P., Bang, M.L., Segnalini, P., Gu, Y., Dalton, N.D., et al. (2007). MicroRNA-133 controls cardiac hypertrophy. Nat. Med. *13*, 613–618.
22. Ebert, M.S., and Sharp, P.A. (2010). MicroRNA sponges: progress and possibilities. RNA *16*, 2043–2050.
23. Caporali, A., Meloni, M., Völlenkle, C., Bonci, D., Sala-Newby, G.B., Addis, R., Spinetti, G., Losa, S., Masson, R., Baker, A.H., et al. (2011). Deregulation of microRNA-503 contributes to diabetes mellitus-induced impairment of endothelial function and reparative angiogenesis after limb ischemia. Circulation *123*, 282–291.
24. Caporali, A., Meloni, M., Nailor, A., Mitić, T., Shantikumar, S., Riu, F., Sala-Newby, G.B., Rose, L., Besnier, M., Katare, R., et al. (2015). p75(NTR)-dependent activation of NF-κB regulates microRNA-503 transcription and pericyte-endothelial crosstalk in diabetes after limb ischaemia. Nat. Commun. *6*, 8024.

25. Horie, T., Ono, K., Nishi, H., Iwanaga, Y., Nagao, K., Kinoshita, M., Kuwabara, Y., Takanabe, R., Hasegawa, K., Kita, T., and Kimura, T. (2009). MicroRNA-133 regulates the expression of GLUT4 by targeting KLF15 and is involved in metabolic control in cardiac myocytes. Biochem. Biophys. Res. Commun. *389*, 315–320.

26. Xie, J., Ameres, S.L., Friedline, R., Hung, J.H., Zhang, Y., Xie, Q., Zhong, L., Su, Q., He, R., Li, M., et al. (2012). Long-term, efficient inhibition of microRNA function in mice using rAAV vectors. Nat. Methods *9*, 403–409.

27. Mullokandov, G., Baccarini, A., Ruzo, A., Jayaprakash, A.D., Tung, N., Israelow, B., Evans, M.J., Sachidanandam, R., and Brown, B.D. (2012). High-throughput assessment of microRNA activity and function using microRNA sensor and decoy libraries. Nat. Methods *9*, 840–846.

28. Wu, J.C., Sundaresan, G., Iyer, M., and Gambhir, S.S. (2001). Noninvasive optical imaging of firefly luciferase reporter gene expression in skeletal muscles of living mice. Mol. Ther. *4*, 297–306.

29. Riegler, J., Gillich, A., Shen, Q., Gold, J.D., and Wu, J.C. (2014). Cardiac tissue slice transplantation as a model to assess tissue-engineered graft thickness, survival, and function. Circulation *130* (11, Suppl 1), S77–S86.

30. Greco, S., Gaetano, C., and Martelli, F. (2014). HypoxamiR regulation and function in ischemic cardiovascular diseases. Antioxid. Redox Signal. *21*, 1202–1219.

31. He, Q., Ren, X., Chen, J., Li, Y., Tang, X., Wen, X., Yang, X., Zhang, J., Wang, Y., Ma, J., and Liu, N. (2016). miR-16 targets fibroblast growth factor 2 to inhibit NPC cell proliferation and invasion via PI3K/AKT and MAPK signaling pathways. Oncotarget *7*, 3047–3058.

32. Schelch, K., Kirschner, M.B., Williams, M., Cheng, Y.Y., van Zandwijk, N., Grusch, M., and Reid, G. (2018). A link between the fibroblast growth factor axis and the miR-16 family reveals potential new treatment combinations in mesothelioma. Mol. Oncol. *12*, 58–73.

33. Quann, K., Jing, Y., and Rigoutsos, I. (2015). Post-transcriptional regulation of BRCA1 through its coding sequence by the miR-15/107 group of miRNAs. Front. Genet. *6*, 242.

34. Nelson, P.T., Wang, W.X., Mao, G., Wilfred, B.R., Xie, K., Jennings, M.H., Gao, Z., and Wang, X. (2011). Specific sequence determinants of miR-15/107 microRNA gene group targets. Nucleic Acids Res. *39*, 8163–8172.

35. Suri, C., Jones, P.F., Patan, S., Bartunkova, S., Maisonpierre, P.C., Davis, S., Sato, T.N., and Yancopoulos, G.D. (1996). Requisite role of angiopoietin-1, a ligand for the TIE2 receptor, during embryonic angiogenesis. Cell *87*, 1171–1180.

36. Jeltsch, M., Leppänen, V.M., Saharinen, P., and Alitalo, K. (2013). Receptor tyrosine kinase-mediated angiogenesis. Cold Spring Harb. Perspect. Biol. *5*, 5.

37. Biel, N.M., and Siemann, D.W. (2016). Targeting the Angiopoietin-2/Tie-2 axis in conjunction with VEGF signal interference. Cancer Lett. *380*, 525–533.

38. Gerald, D., Chintharlapalli, S., Augustin, H.G., and Benjamin, L.E. (2013). Angiopoietin-2: an attractive target for improved antiangiogenic tumor therapy. Cancer Res. *73*, 1649–1657.

39. Eklund, L., Kangas, J., and Saharinen, P. (2017). Angiopoietin-Tie signalling in the cardiovascular and lymphatic systems. Clin. Sci. (Lond.) *131*, 87–103.

40. Fagiani, E., and Christofori, G. (2013). Angiopoietins in angiogenesis. Cancer Lett. *328*, 18–26.

41. Hausser, J., Syed, A.P., Bilen, B., and Zavolan, M. (2013). Analysis of CDS-located miRNA target sites suggests that they can effectively inhibit translation. Genome Res. *23*, 604–615.

42. Leppänen, V.M., Saharinen, P., and Alitalo, K. (2017). Structural basis of Tie2 activation and Tie2/Tie1 heterodimerization. Proc. Natl. Acad. Sci. USA *114*, 4376–4381.

43. Hasenstein, J.R., Kasmerchak, K., Buehler, D., Hafez, G.R., Cleary, K., Moody, J.S., and Kozak, K.R. (2012). Efficacy of Tie2 receptor antagonism in angiosarcoma. Neoplasia *14*, 131–140.

44. Varu, V.N., Hogg, M.E., and Kibbe, M.R. (2010). Critical limb ischemia. J. Vasc. Surg. *51*, 230–241.

45. Pekarsky, Y., Balatti, V., and Croce, C.M. (2018). BCL2 and miR-15/16: from gene discovery to treatment. Cell Death Differ. *25*, 21–26.

46. Aqeilan, R.I., Calin, G.A., and Croce, C.M. (2010). miR-15a and miR-16-1 in cancer: discovery, function and future perspectives. Cell Death Differ. *17*, 215–220.

47. Porrello, E.R., Mahmoud, A.I., Simpson, E., Johnson, B.A., Grinsfelder, D., Canseco, D., Mammen, P.P., Rothermel, B.A., Olson, E.N., and Sadek, H.A. (2013). Regulation of neonatal and adult mammalian heart regeneration by the miR-15 family. Proc. Natl. Acad. Sci. USA *110*, 187–192.

48. Hullinger, T.G., Montgomery, R.L., Seto, A.G., Dickinson, B.A., Semus, H.M., Lynch, J.M., Dalby, C.M., Robinson, K., Stack, C., Latimer, P.A., et al. (2012). Inhibition of miR-15 protects against cardiac ischemic injury. Circ. Res. *110*, 71–81.

49. Xue, G., Yan, H.L., Zhang, Y., Hao, L.Q., Zhu, X.T., Mei, Q., and Sun, S.H. (2015). c-Myc-mediated repression of miR-15-16 in hypoxia is induced by increased HIF-2α and promotes tumor angiogenesis and metastasis by upregulating FGF2. Oncogene *34*, 1393–1406.

50. Rey, S., Schito, L., Wouters, B.G., Eliasof, S., and Kerbel, R.S. (2017). Targeting Hypoxia-Inducible Factors for Antiangiogenic Cancer Therapy. Trends Cancer *3*, 529–541.

51. Augustin, H.G., Koh, G.Y., Thurston, G., and Alitalo, K. (2009). Control of vascular morphogenesis and homeostasis through the angiopoietin-Tie system. Nat. Rev. Mol. Cell Biol. *10*, 165–177.

52. Peters, K.G., Kontos, C.D., Lin, P.C., Wong, A.L., Rao, P., Huang, L., Dewhirst, M.W., and Sankar, S. (2004). Functional significance of Tie2 signaling in the adult vasculature. Recent Prog. Horm. Res. *59*, 51–71.

53. Thurston, G., and Daly, C. (2012). The complex role of angiopoietin-2 in the angiopoietin-tie signaling pathway. Cold Spring Harb. Perspect. Med. *2*, a006550.

54. Shyu, K.G., Manor, O., Magner, M., Yancopoulos, G.D., and Isner, J.M. (1998). Direct intramuscular injection of plasmid DNA encoding angiopoietin-1 but not angiopoietin-2 augments revascularization in the rabbit ischemic hindlimb. Circulation *98*, 2081–2087.

55. Lekas, M., Lekas, P., Mei, S.H., Deng, Y., Dumont, D.J., and Stewart, D.J. (2012). Tie2-dependent neovascularization of the ischemic hindlimb is mediated by angiopoietin-2. PLoS ONE *7*, e43568.

56. Lewis, B.P., Burge, C.B., and Bartel, D.P. (2005). Conserved seed pairing, often flanked by adenosines, indicates that thousands of human genes are microRNA targets. Cell *120*, 15–20.

57. Xu, J., Zhang, R., Shen, Y., Liu, G., Lu, X., and Wu, C.I. (2013). The evolution of evolvability in microRNA target sites in vertebrates. Genome Res. *23*, 1810–1816.

58. Guojing, L., Zhang, R., Xu, J., Wu, C.I., and Lu, X. (2015). Functional Conservation of Both CDS- and 3′-UTR-Located MicroRNA Binding Sites between Species. Mol. Biol. Evol. *32*, 3276.

59. Cloonan, N. (2015). Re-thinking miRNA-mRNA interactions: intertwining issues confound target discovery. BioEssays *37*, 379–388.

60. Erhard, F., Haas, J., Lieber, D., Malterer, G., Jaskiewicz, L., Zavolan, M., Dölken, L., and Zimmer, R. (2014). Widespread context dependency of microRNA-mediated regulation. Genome Res. *24*, 906–919.

61. Eding, J.E., Demkes, C.J., Lynch, J.M., Seto, A.G., Montgomery, R.L., Semus, H.M., Jackson, A.L., Isabelle, M., Chimenti, S., and van Rooij, E. (2017). The Efficacy of Cardiac Anti-miR-208a Therapy Is Stress Dependent. Mol. Ther. *25*, 694–704.

62. Gödény, I., Pollesello, P., Edes, I., Papp, Z., and Bagi, Z. (2013). Levosimendan and its metabolite OR-1896 elicit KATP channel-dependent dilation in resistance arteries in vivo. Pharmacol. Rep. *65*, 1304–1310.

63. Anversa, P., and Capasso, J.M. (1991). Loss of intermediate-sized coronary arteries and capillary proliferation after left ventricular failure in rats. Am. J. Physiol. *260*, H1552–H1560.

64. Carmeliet, P. (2000). Mechanisms of angiogenesis and arteriogenesis. Nat. Med. *6*, 389–395.

65. Hernandez, R., Orbay, H., and Cai, W. (2013). Molecular imaging strategies for in vivo tracking of microRNAs: a comprehensive review. Curr. Med. Chem. *20*, 3594–3603.

66. Ylä-Herttuala, S., Bridges, C., Katz, M.G., and Korpisalo, P. (2017). Angiogenic gene therapy in cardiovascular diseases: dream or vision? Eur. Heart J. *38*, 1365–1371.

67. Emanueli, C., Salis, M.B., Stacca, T., Gaspa, L., Chao, J., Chao, L., Piana, A., and Madeddu, P. (2001). Rescue of impaired angiogenesis in spontaneously hypertensive rats by intramuscular human tissue kallikrein gene transfer. Hypertension *38*, 136–141.

68. Mitić, T., Caporali, A., Floris, I., Meloni, M., Marchetti, M., Urrutia, R., Angelini, G.D., and Emanueli, C. (2015). EZH2 modulates angiogenesis in vitro and in a mouse model of limb ischemia. Mol. Ther. *23*, 32–42.

69. Bindea, G., Mlecnik, B., Hackl, H., Charoentong, P., Tosolini, M., Kirilovsky, A., Fridman, W.H., Pagès, F., Trajanoski, Z., and Galon, J. (2009). ClueGO: a Cytoscape plug-in to decipher functionally grouped gene ontology and pathway annotation networks. Bioinformatics *25*, 1091–1093.

70. Bonci, D., Coppola, V., Musumeci, M., Addario, A., Giuffrida, R., Memeo, L., D'Urso, L., Pagliuca, A., Biffoni, M., Labbaye, C., et al. (2008). The miR-15a-miR-16-1 cluster controls prostate cancer by targeting multiple oncogenic activities. Nat. Med. *14*, 1271–1277.

71. Sala-Newby, G.B., Freeman, N.V., Curto, M.A., and Newby, A.C. (2003). Metabolic and functional consequences of cytosolic 5′-nucleotidase-IA overexpression in neonatal rat cardiomyocytes. Am. J. Physiol. Heart Circ. Physiol. *285*, H991–H998.

72. Cao, F., Lin, S., Xie, X., Ray, P., Patel, M., Zhang, X., Drukker, M., Dylla, S.J., Connolly, A.J., Chen, X., et al. (2006). In vivo visualization of embryonic stem cell survival, proliferation, and migration after cardiac delivery. Circulation *113*, 1005–1014.

OMTN, Volume *17*

Supplemental Information

miR-15a/-16 Inhibit Angiogenesis by Targeting the Tie2 Coding Sequence: Therapeutic Potential of a miR-15a/16 Decoy System in Limb Ischemia

Marie Besnier, Saran Shantikumar, Maryam Anwar, Parul Dixit, Aranzazu Chamorro-Jorganes, Walid Sweaad, Graciela Sala-Newby, Paolo Madeddu, Anita C. Thomas, Lynsey Howard, Sobia Mushtaq, Enrico Petretto, Andrea Caporali, and Costanza Emanueli

Supplementary figure S1

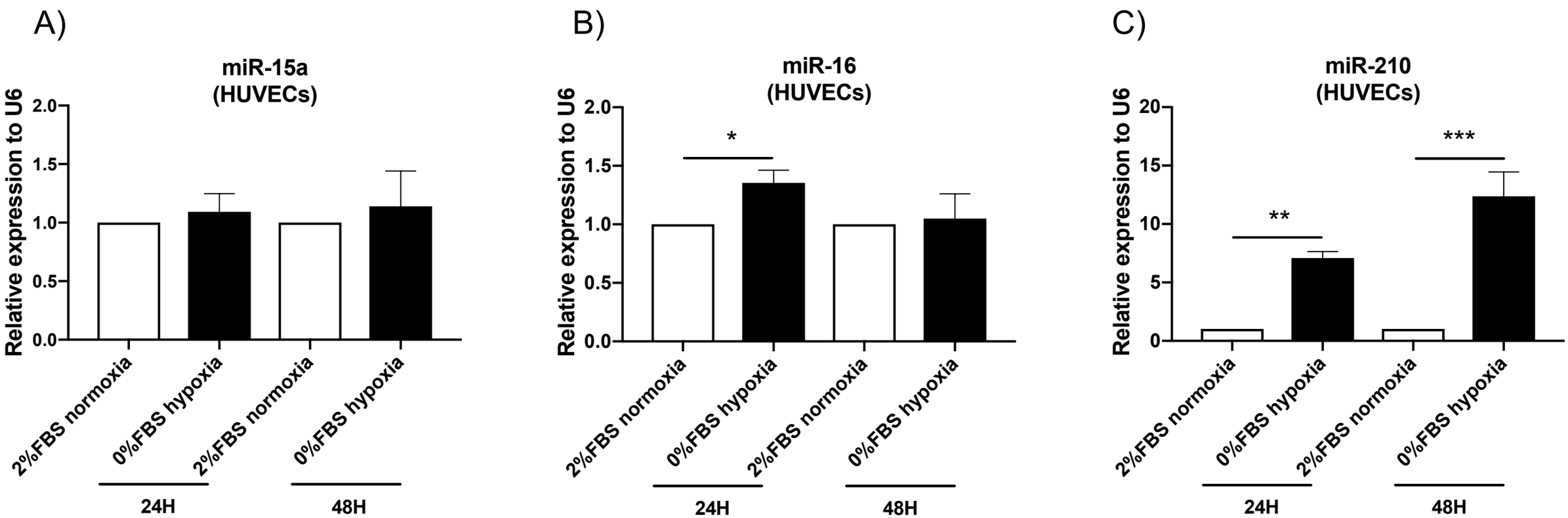

Supplementary figure S2

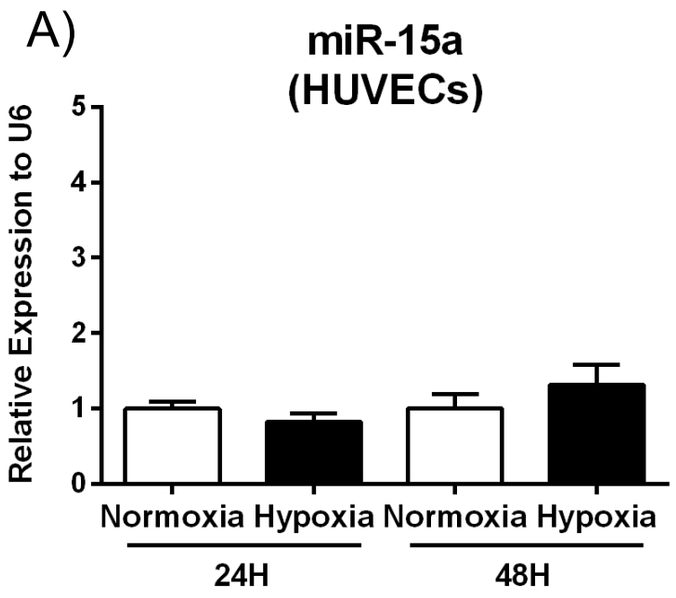

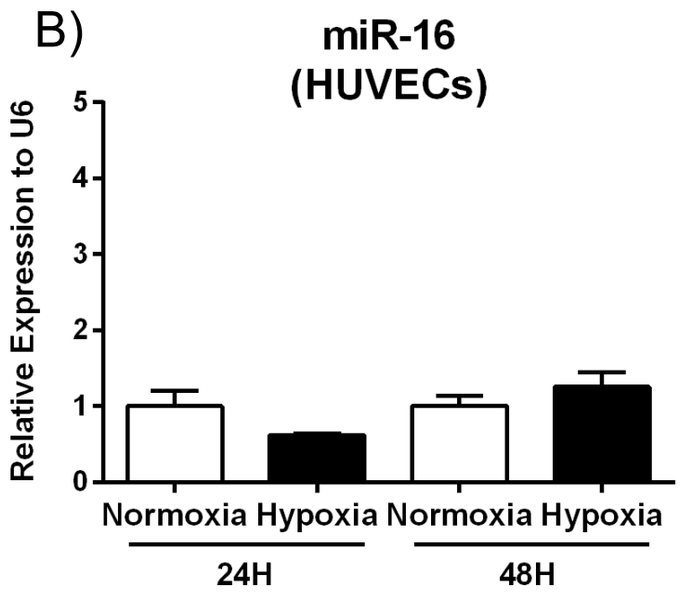

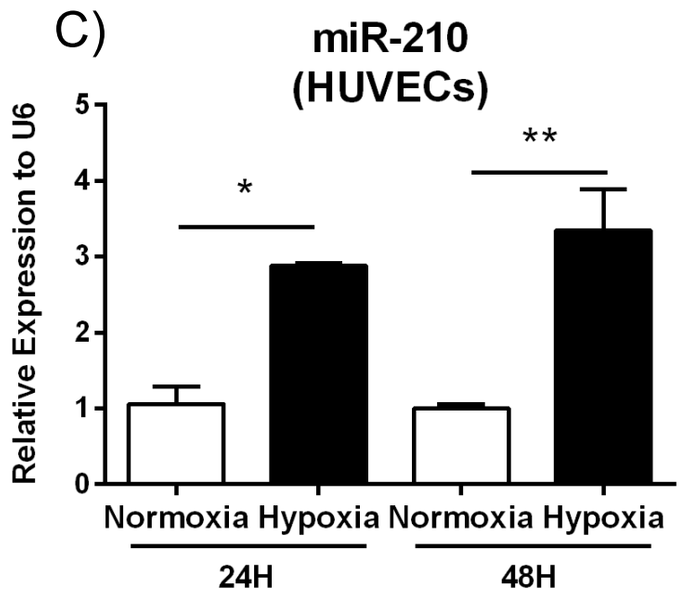

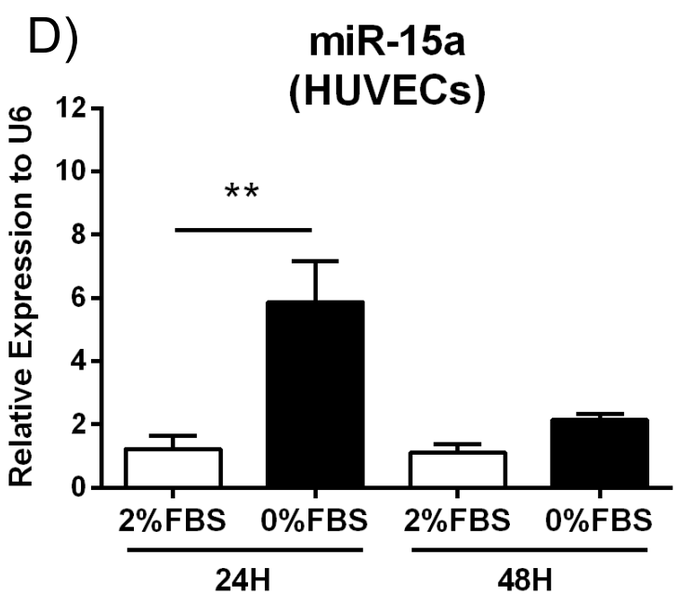

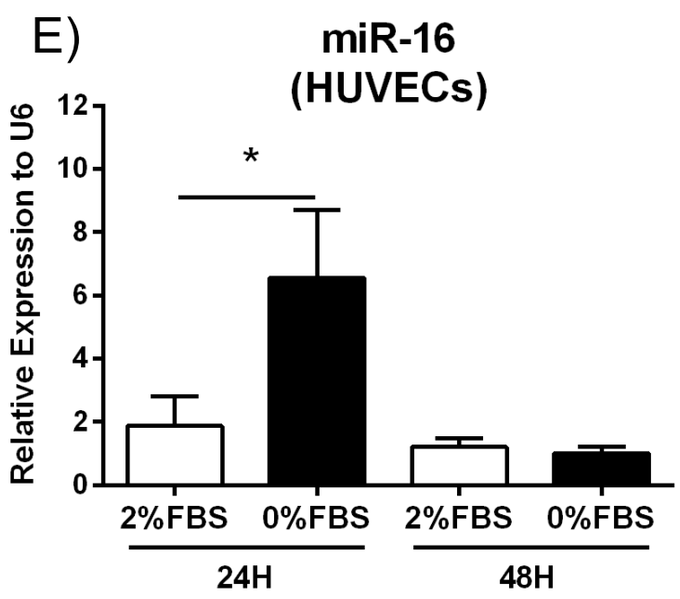

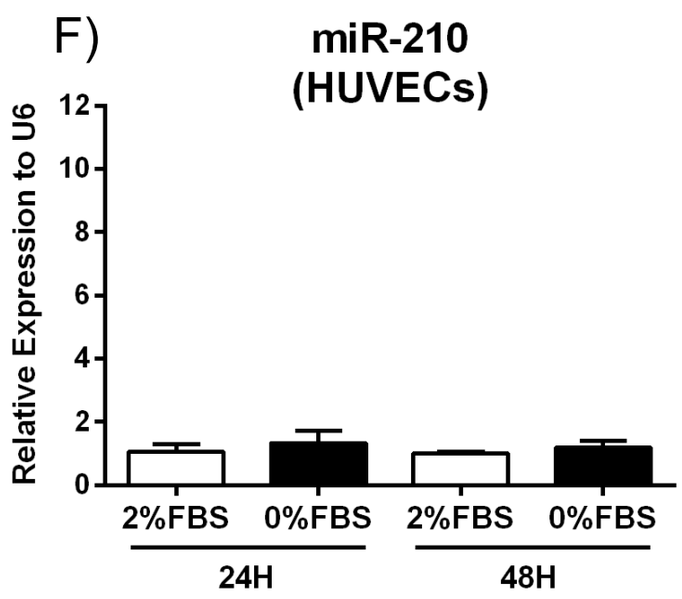

Supplementary figure S3

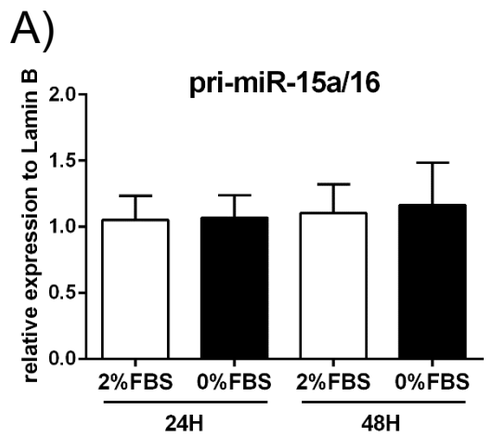

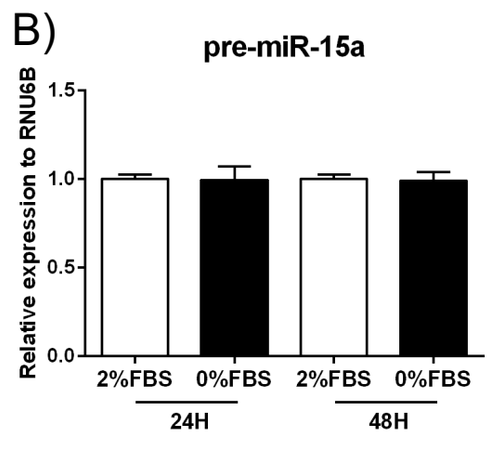

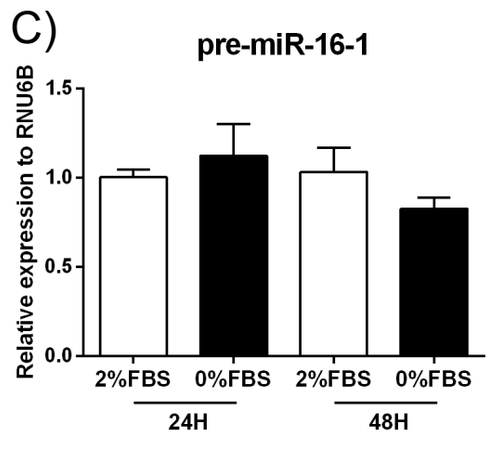

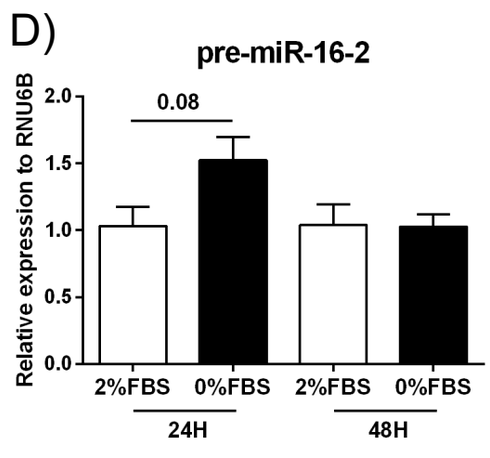

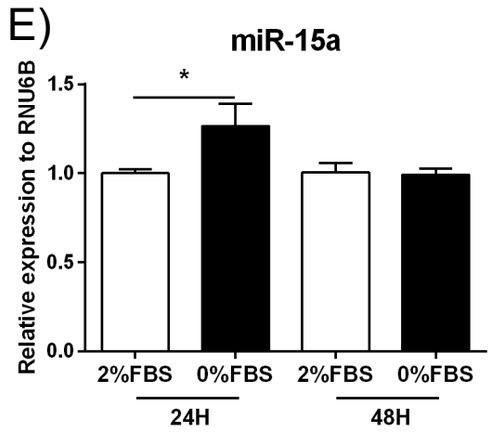

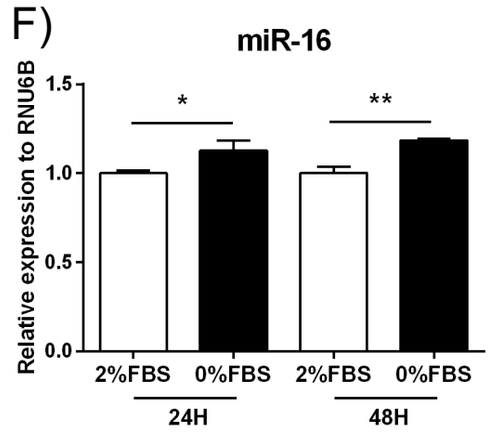

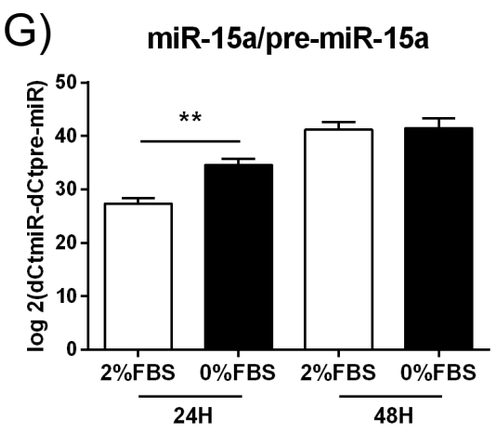

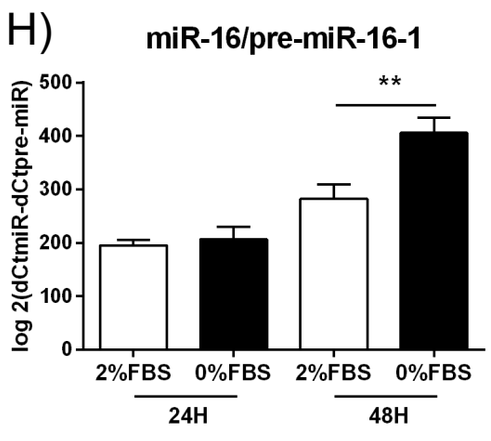

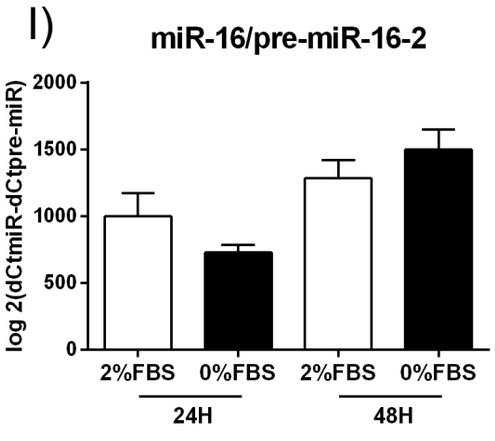

Supplementary figure S4

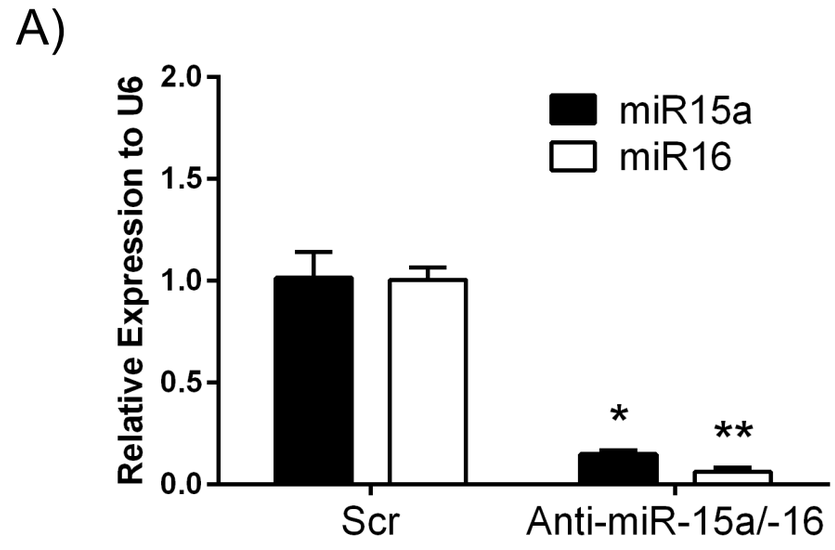

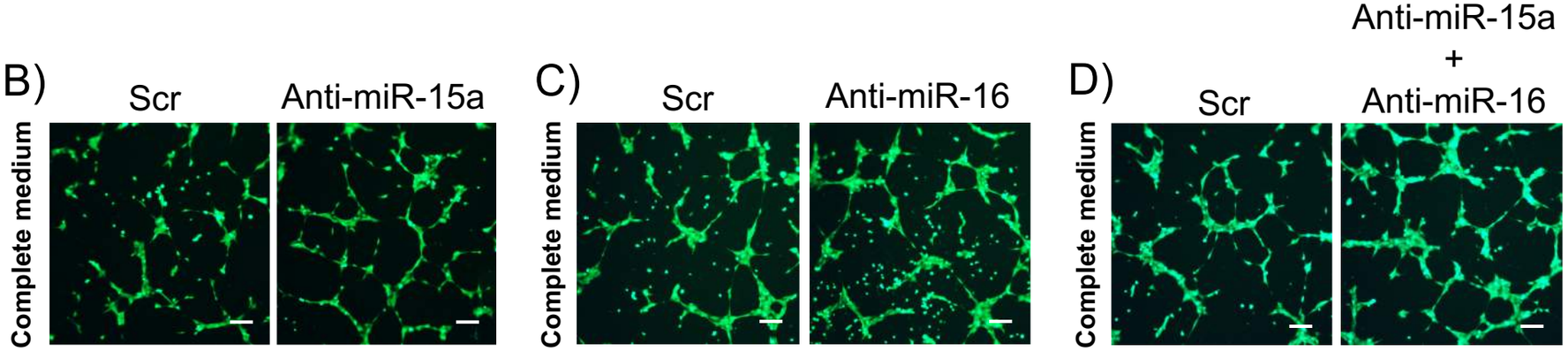

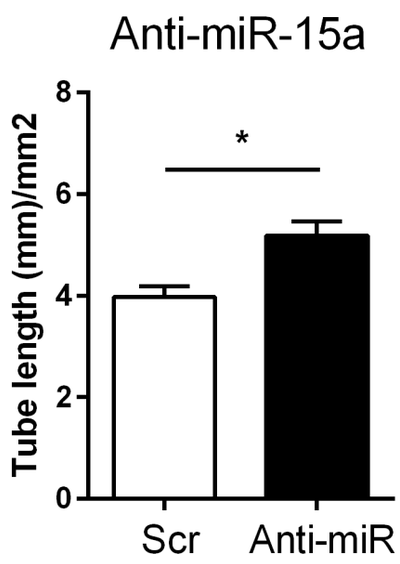

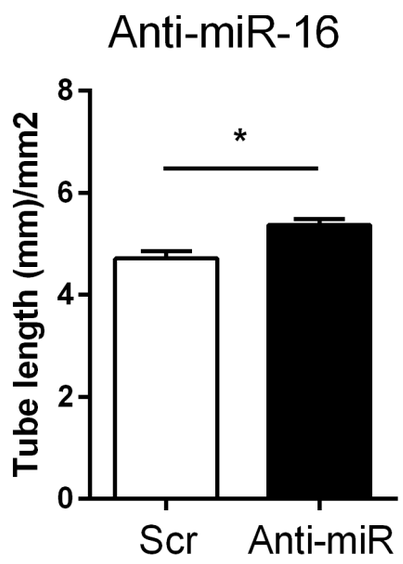

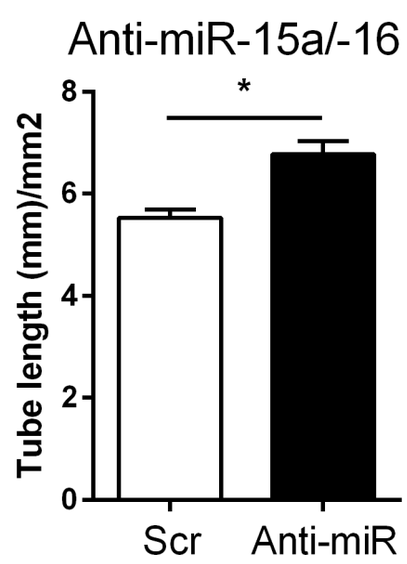

Supplementary figure S5

A)

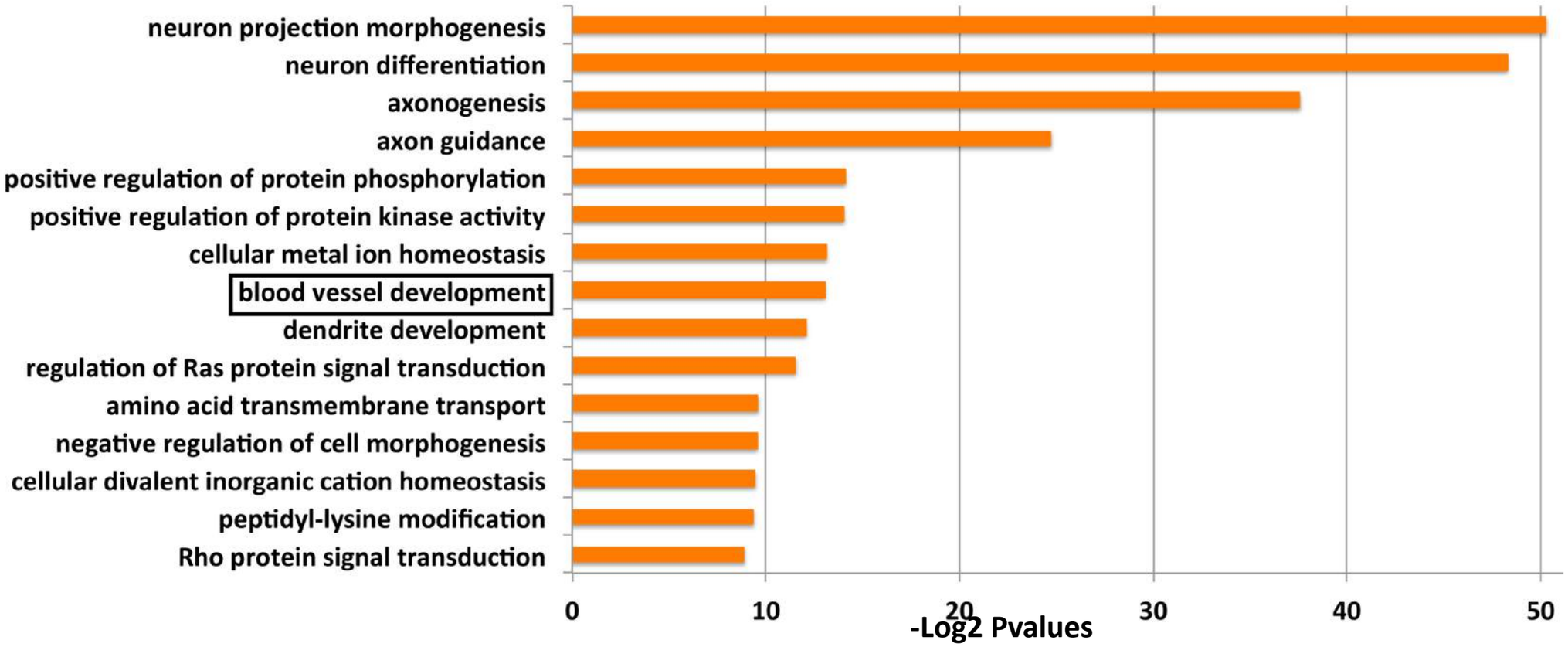

B)

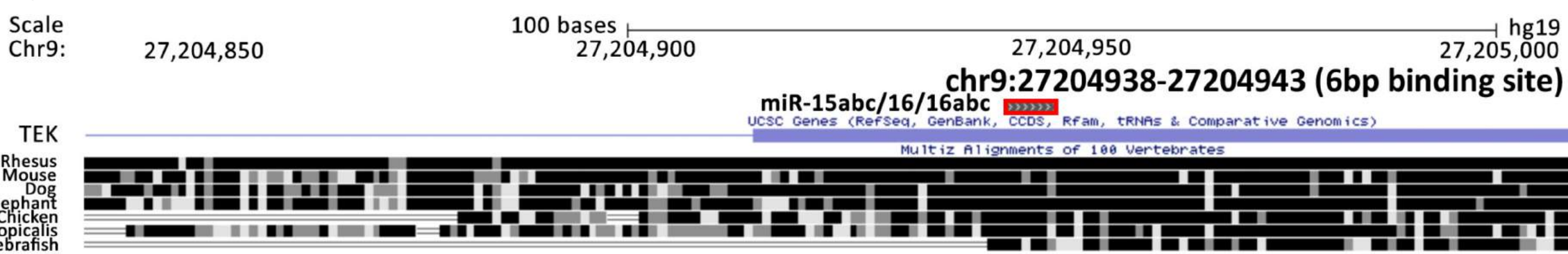

C)

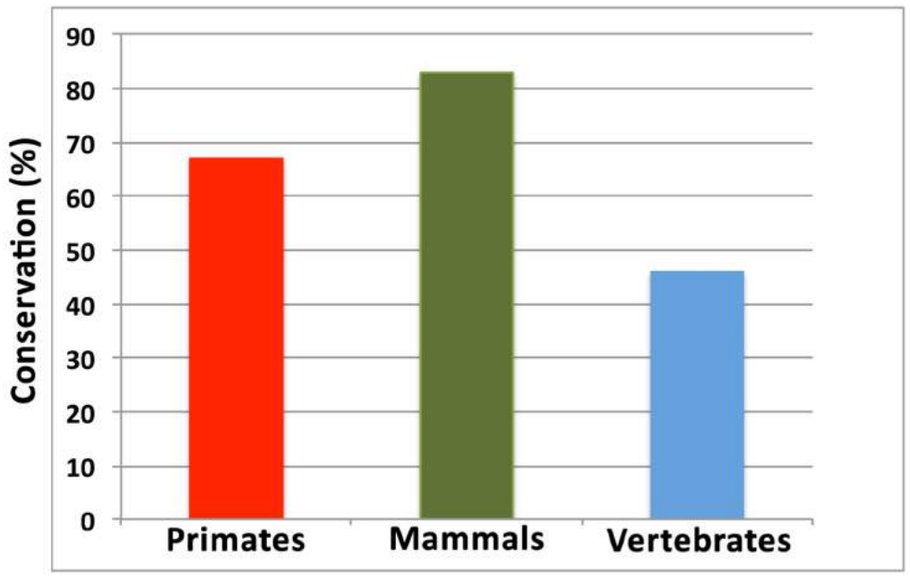

Supplementary figure S6

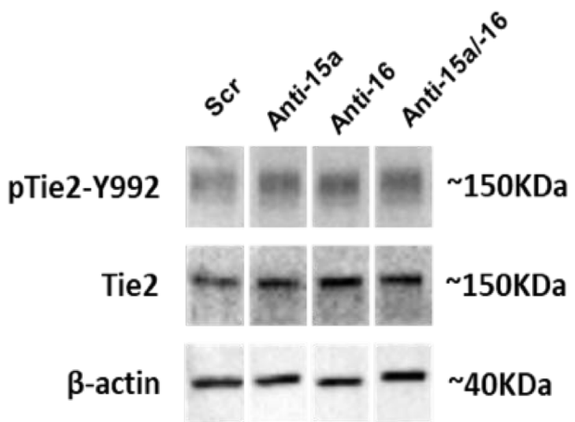

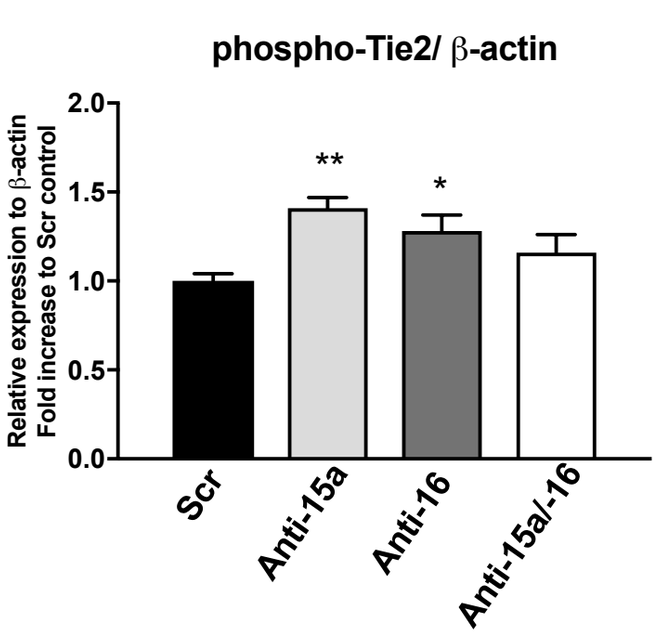

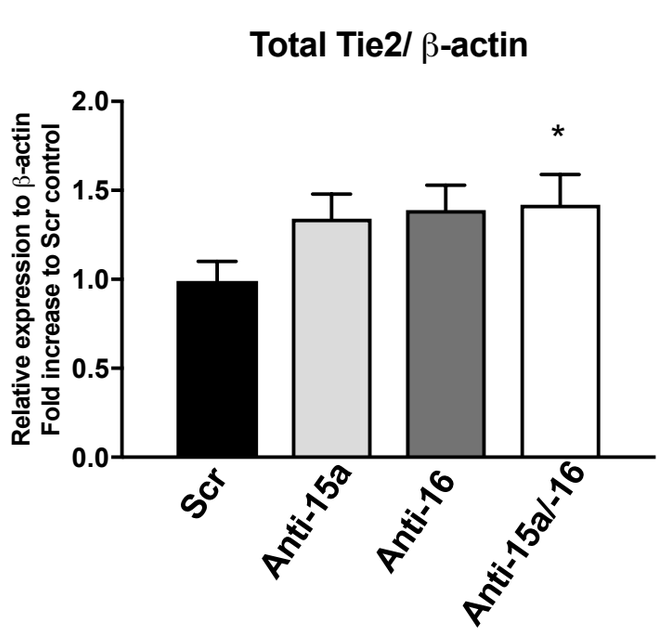

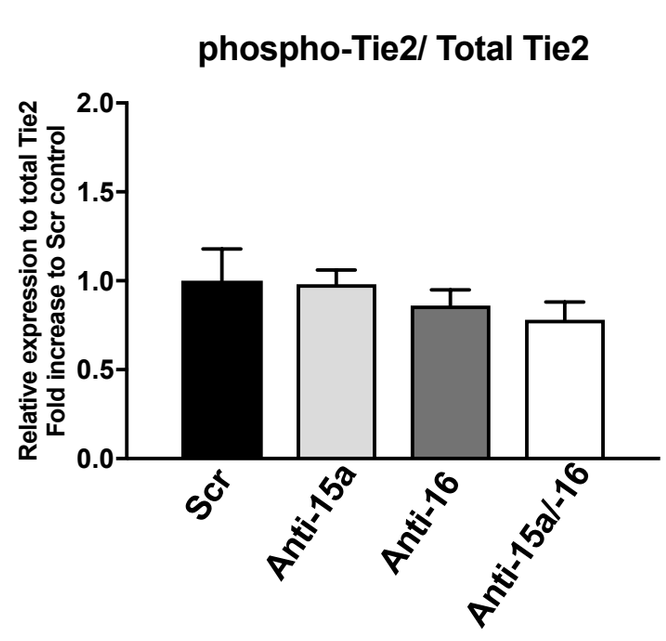

Supplementary figure S7

A)

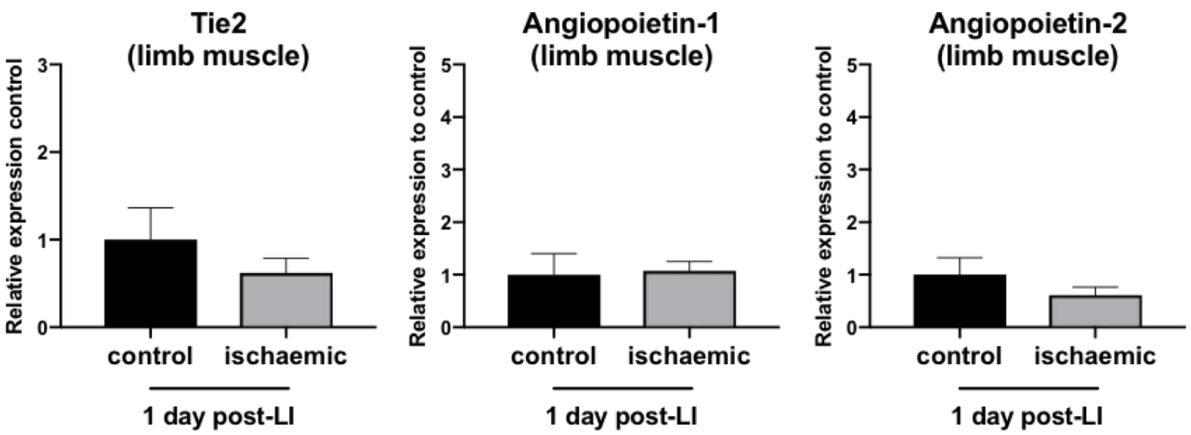

B)

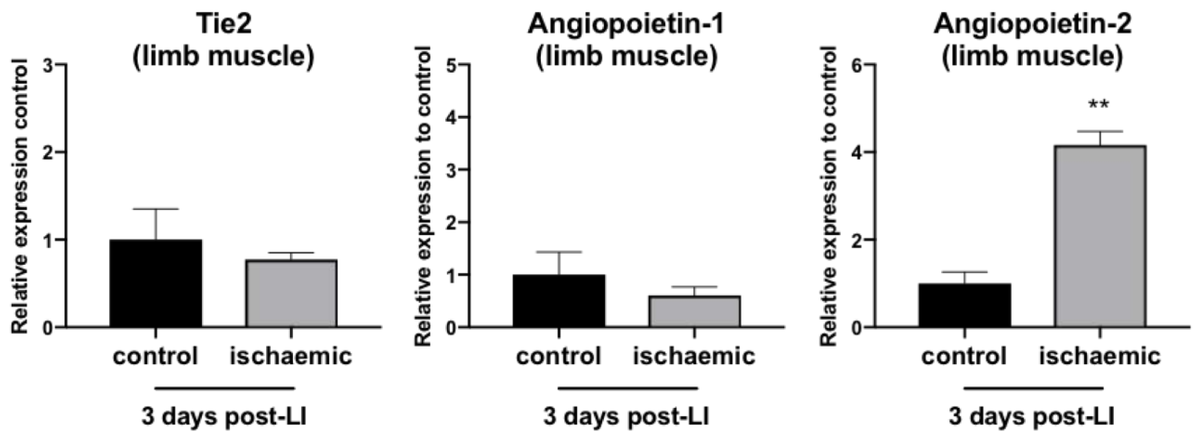

C)

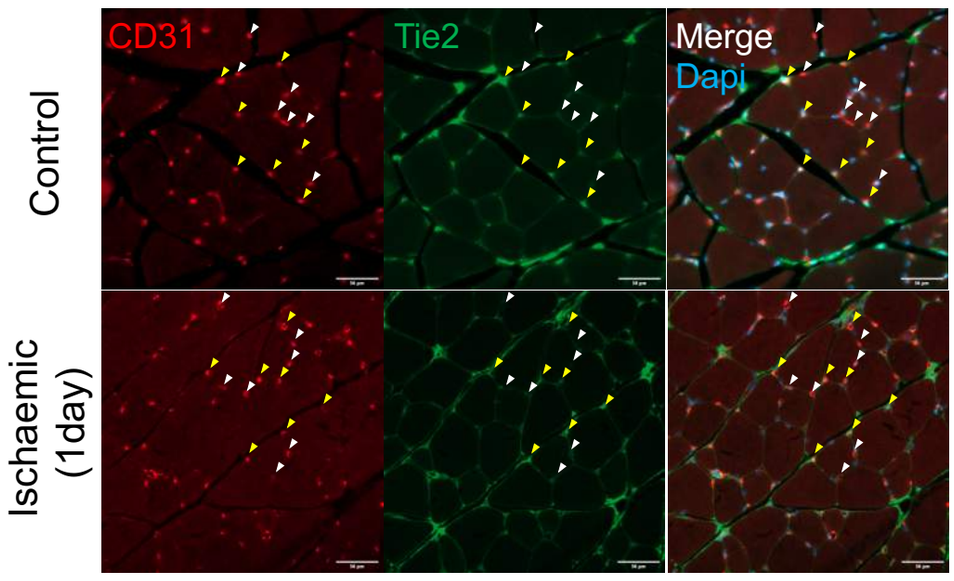

F)

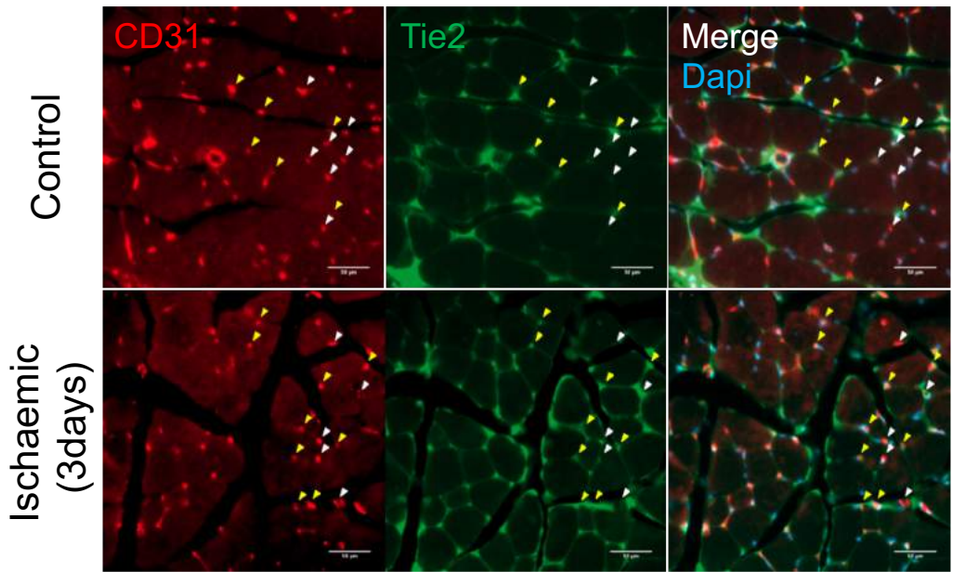

D)

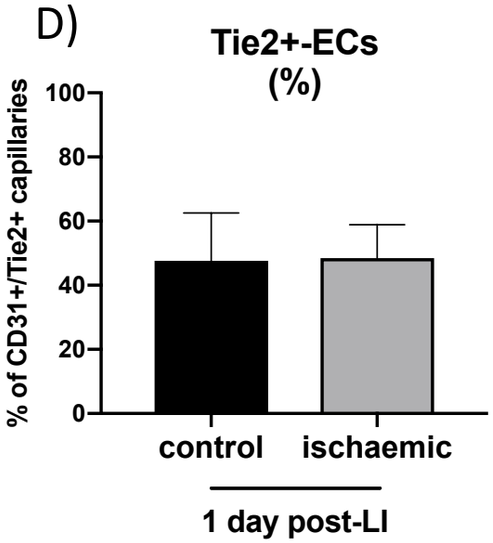

E)

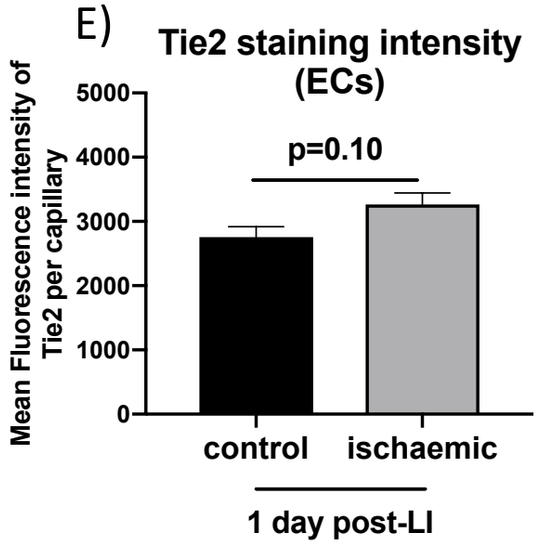

G)

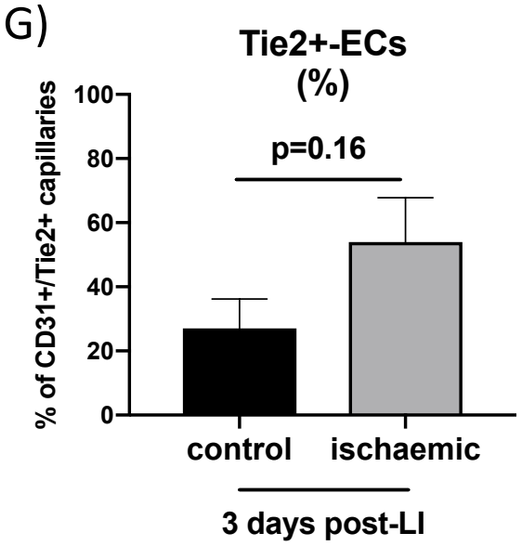

H)

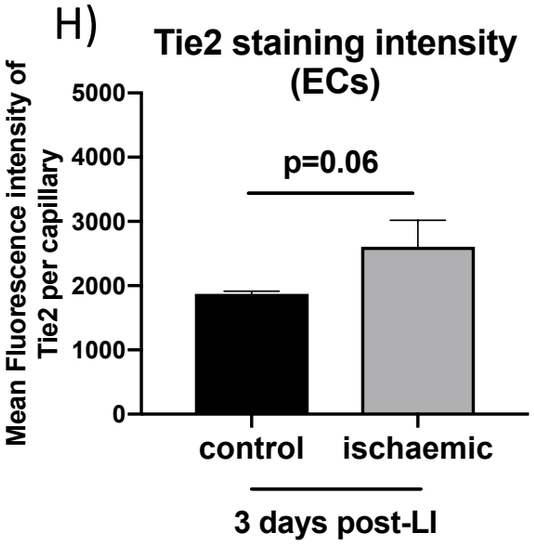

Supplementary figure S8

A)

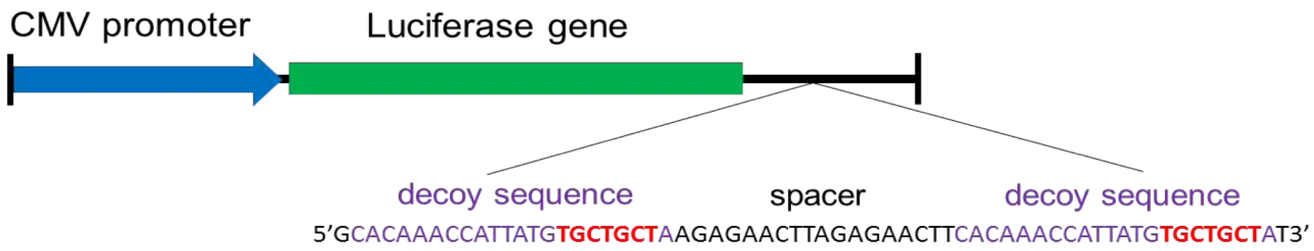

	"seed"
miR-15a	5'-UAGCAGCACAUAAUGGUUUGUG-3'
miR-16	5'-UAGCAGCACGUAAAUAUUGGCG-3'
miR-15b	5'-UAGCAGCACAUCAUGGUUUACA-3'
miR-503	5'-UAGCAGCGGGAACAGUUCUGCAG-3'

B)

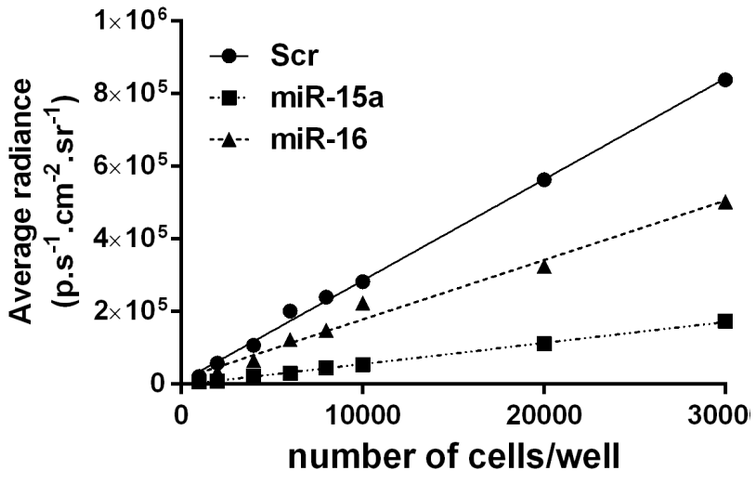

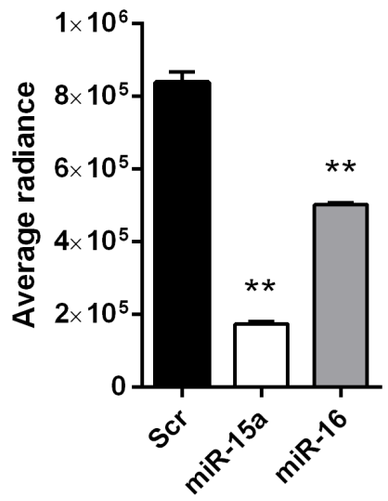

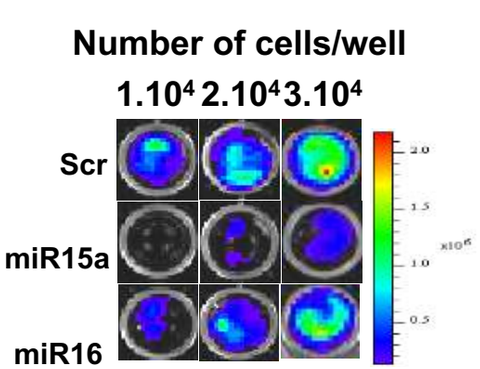

C)

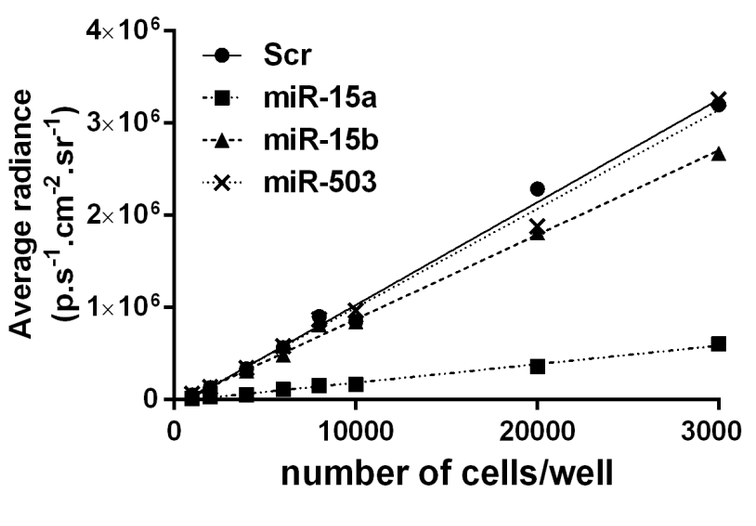

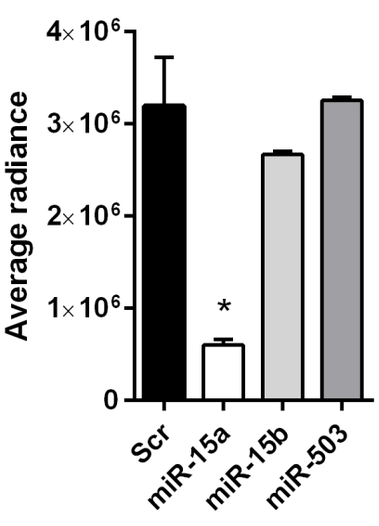

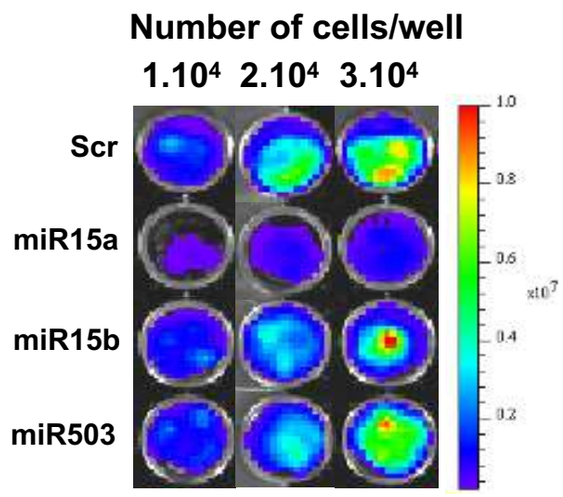

Supplementary figure S9

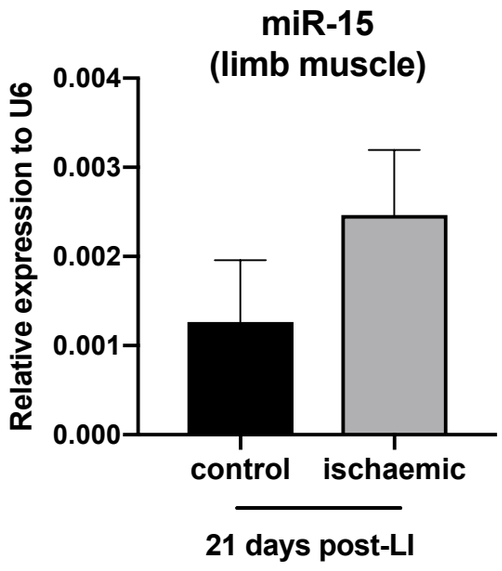

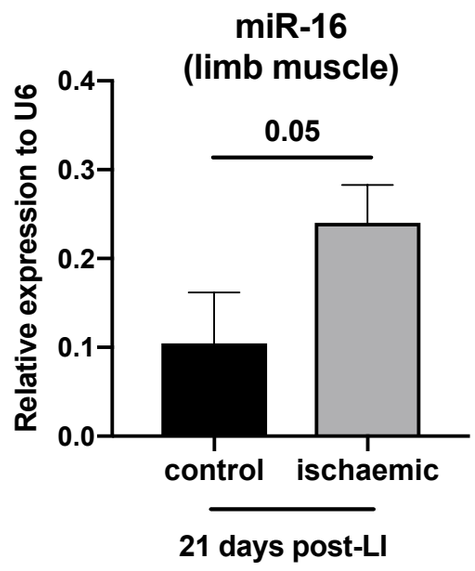

Supplementary figure S10

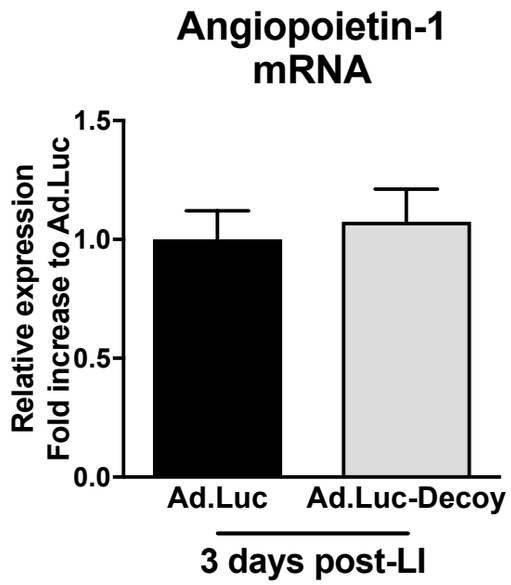

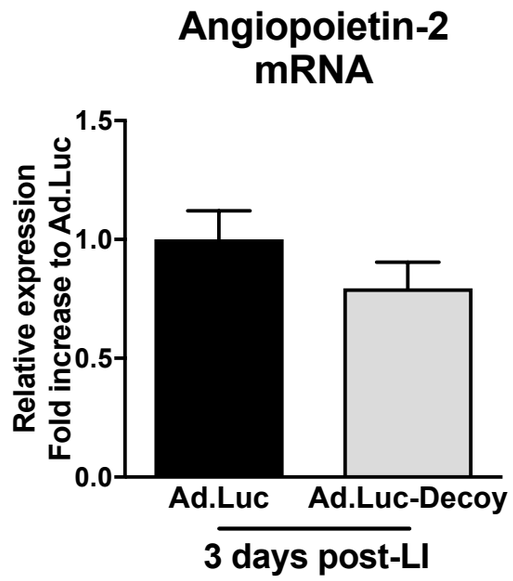

Supplementary figure S11

A)

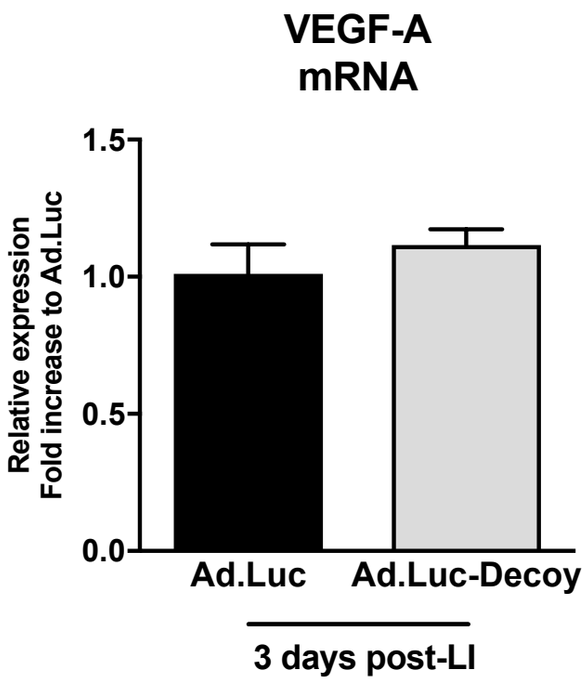

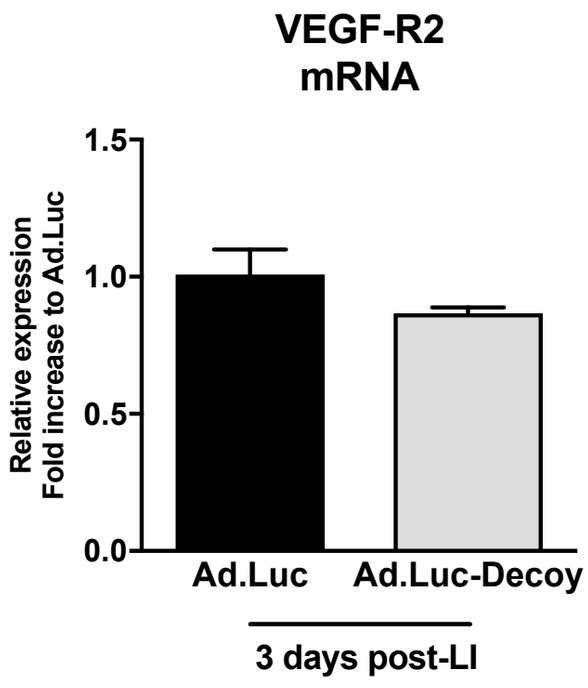

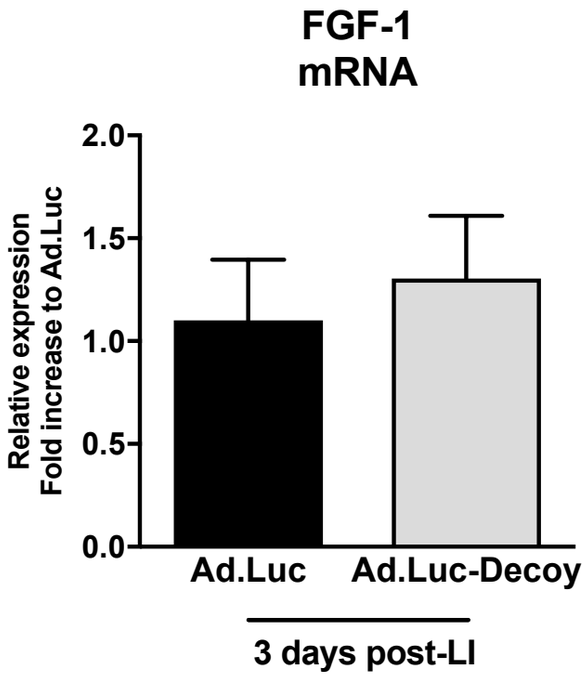

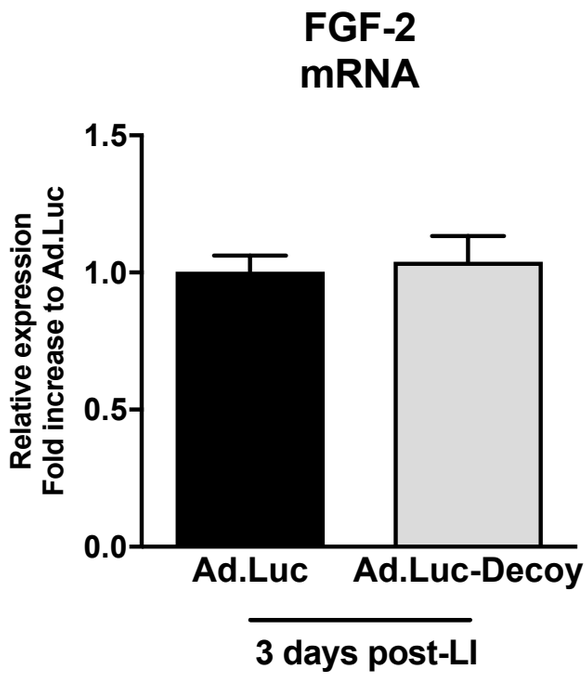

B)

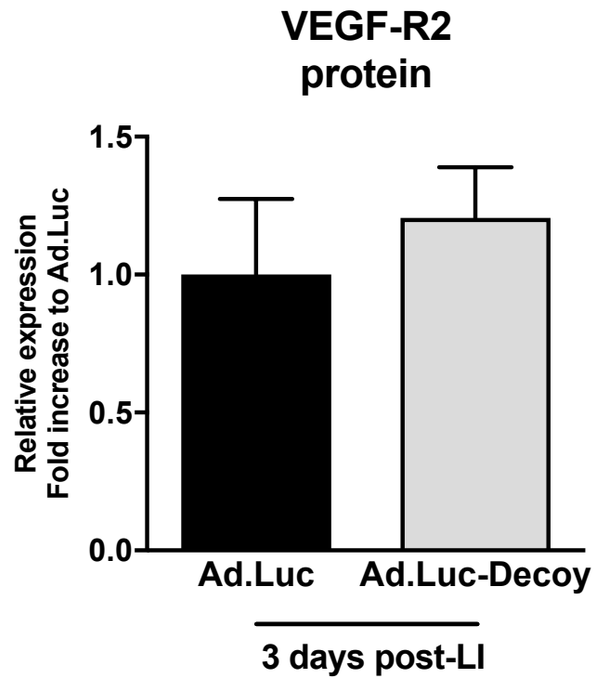

Supplemental data

Supplementary figure S1 : Expression of miR-16 and -210 in HUVECs is affected by hypoxia associated to serum deprivation, in opposition to miR-15a expression.

MiR-15a (A), -16 (B) and -210 (C) expressions were evaluated using RT-PCR in Human Umbilical Vein Endothelial Cells (HUVECs) cultured under normoxic and Foetal Bovine Serum (FBS)-complete (2% FBS) medium or hypoxic and FBS-free (0% FBS) medium for 24 or 48 h. Results were normalized to the small nuclear RNA U6 expression. Results are presented as mean ± SEM. n=3 per condition, *p < 0.05, **p < 0.01 and *** *p* < 0.001 *versus* time-matched normoxic and 2% FBS medium conditions.

Supplementary figure S2 : Expression of miR-15a and -16 in HUVECs is affected by serum deprivation but not by hypoxia, in contrast to hypoxamiR-210 expression.

MiR-15a, -16 and -210 expressions were evaluated using RT-PCR in Human Umbilical Vein Endothelial Cells (HUVECs) cultured under normoxic/hypoxic conditions (A-C), or Foetal Bovine Serum (FBS)-complete (2% FBS) or FBS-free (0% FBS) media (D-E) for 24 or 48 h. Results were normalized to the small nuclear RNA U6 expression. Results are presented as mean ± SEM. n=3-5 per condition, *p < 0.05 and **p < 0.01 *versus* time-matched normoxic or 2% FBS medium conditions.

Supplementary figure S3 : Increase of miR-15a and -16 in serum deprivation in HUVECs is due to an increase in precursor (pre-miR) maturation, and not an increase of primary transcript (pri-miR) transcription.

The mechanism behind the increased expression of miR-15a and -16 under serum deprivation was assessed in Human Umbilical Vein Endothelial Cells (HUVECs) cultured under Foetal Bovine Serum (FBS)-complete (2% FBS) or FBS-free (0% FBS) media for 24 or 48 h. (A) Expression of the primary transcript pri-miR-15a/-16-1 was measured by RT-PCR and normalized to Lamin B. (B, C, D) The relative expression of the precursors of miR-15a and -16 (pre-miR-15a/-16-1/-16-2) and the mature form of miR-15a (E) and -16 (F) was also measured by RT-PCR and normalized to small nuclear RNU6B. The relative expression of each mature miR compared to their precursors is also shown (G, H, I). Results are presented as mean ± SEM. n=3 per condition. *p < 0.05 , **p < 0.01 *versus* time-matched 2% FBS medium condition.

Supplementary figure S4 : MiR-15a and/or -16 inhibition decreases HUVEC tube formation on Matrigel assay.

Human Umbilical Vein Endothelial Cells HUVECs were transfected with a Scramble oligo (Scr) or an anti-miR against miR-15a or miR-16, or the two anti-miRs together (total concentration of 20 nM) to inhibit their activity. MiR-15a and miR-16 expression after anti-miR transfection in HUVECs was assessed using RT-PCR and normalized to small nuclear U6 (A). The angiogenic capacity of HUVECs (measured by network formation on Matrigel) after inhibition of miR-15a (B), miR-16 (C) and both miR-15a and -16 (D) was assessed and is presented as tube length (mm) per mm^2. Representative images of each condition are provided showing, in green, HUVECs stained with Calcein, 6 h after plating the cells on Matrigel. Scale bar: 100 µm. All experiments were performed in triplicate with n=3 per condition. All data are expressed as mean ± SEM. *p < 0.05 , **p < 0.01 vs. Scr-control.

Supplementary figure S5 : Bioinformatic analysis of potential targets of miR-15a and -16 involved in angiogenesis, positions of miR-15a and -16 seed sequence binding on the human sequence of *TEK* on chromosome 9, and validation of the target.

Predicted common targets of miR15/16 obtained from miRcode were subjected to gene ontology (GO) analysis using the program CLUEGO. (A) The top 15 significantly enriched GO terms are shown as a bar graph, with the x-axis indicating $-\log_2$ (p values) and significant GO terms on the y-axis. Higher values indicate greater statistical significance. An interesting term is "blood vessel development" that corresponds to 415 target genes. (B) miRcode results reveal that one of these 415 target genes is "*TEK*" which has a 6 bp binding site for miR15/16 in its coding sequence (shown in the UCSC browser highlighted in red) at position chr9: 27204938-27204943. At the bottom of the browser are Multiz alignments of 100 vertebrates, which indicate conservation as a grey-scale density plot, where darker regions indicate more conservation. (C) This predicted binding site of miR15/16 in the CDS region of *TEK* is most highly conserved in mammals (83%), followed by primates (67%) and vertebrates (46%).

Supplementary figure S6 : MiR-15a and -16 inhibition in HUVECs increases Tie2 expression level leading to an overall increase of Tie2 phosphorylation.

HUVECs were transfected with a Scramble oligo (Scr) or an anti-miR against miR-15a or miR-16, or the two anti-miRs simultaneously (total concentration of 50 nM) to inhibit their activity. Phospho-Tie2 (Y922) and total Tie2 protein expression were assessed by western blot and normalized to β-actin and expressed relatively to Scr condition. Results are presented as mean ± SEM. n=6 for each condition. Representative pictures of cropped WB images are also shown. * $p < 0.05$, ** $p < 0.01$ versus Scr condition.

Supplementary figure S7 : Tie2 and Angiopoietin(Ang)-1 and -2 expression in whole limb muscles and muscle-ECs in our model of limb ischemia.

Tie-2, Ang-1 and Ang-2 expression was evaluated by RT-PCR in control/non-ischemic limb muscles collected at 1 day (A) and 3 days (B) after limb ischemia (LI) induction. (C-H) Tie-2 expression in limb muscle ECs, identified by CD31 marker, was measured using immunohistofluorescence in limb muscle tissues, 1 day and 3 days after LI. (C&F) Representative microphotographs showing co-staining of Tie-2 (green) and CD31 (red) in contralateral (control) muscle and ischemic muscle (n=5 per group). Yellow arrows show Tie-2 positive capillaries (Tie-2+/CD31+) while white arrows show Tie-2 negative capillaries (Tie2-/CD31+). Scale bar: 50 µm. (E&F) The percentage of Tie-2+/CD31+ capillaries was analysed and the intensity of Tie-2 within the Tie-2+/CD31+ capillaries was also reported (G&H). n=4 per condition. Results were presented as mean ± SEM. ** $p < 0.01$, versus control condition.

Supplementary figure S8 : Adenovirus carrying a decoy sequence for miR-15a and -16 (*Ad.Luc-Decoy*), gene construction and inhibition efficiency *in vitro*.

(A) Schematic description of the functional decoy-miR15a/16 vector. The decoy sequence is perfectly complementary to the miR-15a sequence. CMV: cytomegalovirus immediate early promoter. Mature sequences of miR-15a, -15b, -16 and -503 are also provided. Efficiency of the virus has been evaluated in Hela cells infected with *Ad.Luc-Decoy* and transfected either with pre-miR scramble (Scr), pre-miR-15a (miR-15a) and pre-miR-16 (miR-16) at 25 nM (B) or with pre-miR-15b (miR-15b) and pre-miR-503 (miR-503) to investigate the specificity of the construct (C). (B and C) Results show the luciferase activity, measured on a Xenogen In Vivo Imaging System (IVIS), of increasing numbers of cells (1000-30000) plated in 96-well plates. Values obtained with 30000 cells and representative

images acquired with the IVIS system are also presented. Each well picture was cropped as cells were plated non-adjacently to avoid light-crossing between wells. Results are presented as mean ± SEM. Experiments were performed in duplicate, n=2 per condition, and expressed in as photons per second per centimetre-squared per steradian (p. s^{-1}. cm^{-2}.sr^{-1}). *p < 0.05 and **p < 0.01 *versus* the pre-miR Scr condition, Student's *t*-test.

Supplementary figure S9 : Mir-16 expression is increased 21 days after limb ischemia.

At 21 days after limb ischemia surgery, ischemic and non-ischemic/contralateral (control) adductor muscles were collected and the expression of miR-15a and -16 assessed by RT-PCR in the total muscle tissue. Results were normalized to snU6 (n=4-6). Results were expressed relatively to Ad.Luc control condition and presented as mean ± SEM.

Supplementary figure S10 : Inhibition of miR-15a/-16 in vivo does not modify the expression of Tie2 agonist Angiopoietin-1 and Angiopoietin-2 after limb ischemia.

Angiopoietin-1 and Angiopoietin-2 expression in ischemic adductor muscles, 3 days after limb ischemia surgery and injection with either Ad.Luc or Ad.Luc-Decoy virus, was assessed at mRNA level by RT-PCR. Results were normalized to 18S (n=6). Results were expressed relatively to Ad.Luc control condition and presented as mean ± SEM.

Supplementary figure S11 : Inhibition of miR-15a/-16 in vivo does not modify the expression of previously described targets of miR-15a and -16 in our model of limb ischemia.

(A) VEGF-A, VEGF-R2, FGFb, FGF-1 expression in ischemic adductor muscles, 3 days after limb ischemia surgery and injection with either Ad.Luc or Ad.Luc-Decoy virus, was assessed at mRNA level by RT-PCR. Results were normalized to GAPDH (n=3). (B) VEGF-R2 expression in ischemic adductor muscles, 3 days after limb ischemia surgery and injection with either Ad.Luc or Ad.Luc-Decoy virus, was assessed at protein level by western blot. Results were normalized to HSP-90 (n=6) and presented as mean ± SEM.

Supplementary Table 1: Information for probes used in TaqMan-based quantitative real-time PCR assays (Applied Biosystems, UK)

Gene ID	Reference
hsa/mmu-miR-15a	000389
hsa/mmu-miR-15b	000390
hsa/mmu-miR-16	000391
hsa/mmu-miR-503	001048
hsa/mmu-miR-210	000512
snRU6	001973

Supplementary Table 2: Information for primer-pairs used in SYBR Green-based quantitative real-time PCR assays (Sigma and Qiagen)

Gene ID	SEQUENCE
human pri-miR-15a-16-1	forward: 5’-AAGGTGCAGGCCATATTGTG-3’
	reverse: 5’-AAGGCACTGCTGACATTGC-3’
human β-actin	forward: 5’-TGGACATCCGCAAAGACCTGT-3’
	reverse: 5’-GGGCAGTGATCTCCTTCTGCA-3’
human GAPDH	forward: 5’-TGCACCACCAACTGCTTAGC-3’
	reverse: 5’-GGCATGGACTGTGGTCATGAG-3'
human LaminB	forward: 5’-CTGGAAATGTTTGCATCGAAGA-3’
	reverse: 5’-GCCTCCCATTGGTTGATCC-3'
human Tie2	forward: 5’-GGGACCCCACACTTCCAACAA-3’
	reverse: 5’-TTTGGTATCAGCAGGGCTGG-3'
human/mouse 18S	forward: 5’-CCCAGTAAGTGCGGGTCATAA-3'
	reverse: 5’-CCGAGGGCCTCACTAAACC-3'
mouse angiopoietin1	forward: 5’-GGGGGAGGTTGGACAGTAA-3’
	reverse: 5'-CATCAGCTCAATCCTCAGC-3'
mouse angiopoietin2	forward: 5’-GATCTTCCTCCAGCCCCTAC-3’
	reverse: 5'-TTTGTGCTGCTGTCTGGTTC-3'
mouse FGF-1	forward: 5’-AAAGTGCGGGCGAAGTGTA-3’
	reverse: 5'-CTCATTTGGTGTCTGCGAGC-3'
mouse FGFb	forward: 5’-GGCTGCTGGCTTCTAAGTGT-3’
	reverse: 5'-GTCCCGTTTTGGATCCGAGT-3'
mouse VEGF-A	forward: 5’-GGAGATCCTTCGAGGAGCACTT-3’
	reverse: 5'-GGCGATTTAGCAGCAGATATAAGAA-3'
mouse VEGF-R2	forward: 5’-TACAGACCCGGCCAAACAA-3’
	reverse: 5'-TTTCCCCCCTGGAAATCCT-3'
mouse Tie2	forward: 5’-TACAACGGCCATTTCTCCTC-3’
	reverse: 5’-GTGGCTTGCTTGGTACAGGT-3'
miR-15a	forward: 5'-TAGCAGCACATAATGGTTTGTGAAA-3'
miR-16	forward: 5'-TAGCAGCACGTAAATATTGGCGAA-3'
pre-miR-15a	forward : 5'-GCACATAATGGTTTGTGGATTT-3'
pre-miR-16-1	forward : 5'-GTAAATATTGGCGTTAAGATTC-3'
pre-miR-16-2	forward : 5'-GCGTAGTGAAATATATATTAAACACC-3'